Modeling of a Compact Broad-Stopband Lowpass Filter Using Microstrip Stepped Impedance Resonator for Microwave Application

by

Sayed Ashraf Mamun

MASTER OF SCIENCE IN ENGINEERING

Department of Electrical and Electronic Engineering

BANGLADESH UNIVERSITY OF ENGINEERING AND TECHNOLOGY

September 2011

DECLARATION

It is hereby declared that this thesis or any part of it has not been submitted elsewhere for the award of any degree or diploma and all sources are acknowledged.

Sayed Ashraf Mamun

Roll No. 1009062063F

APPROVAL CERTIFICATE

This thesis titled "MODELING OF A COMPACT BROAD-STOPBAND LOWPASS FILTER USING MICROSTRIP STEPPED IMPEDANCE RESONATOR FOR MICROWAVE APPLICATION" submitted by Sayed Ashraf Mamun, Roll No.-1009062063F has been accepted as satisfactory in partial fulfillment of the requirements for the Degree of **Master of Science in Electrical and Electronic Engineering** On 24 September, 2011

BOARD OF EXAMINERS

1.	______________________________ Dr. Md. Abdul Matin Professor Department of Electrical and Electronic Engineering (EEE) Bangladesh University of Engineering and Technology (BUET) Dhaka-1000, Bangladesh	Chairman (Supervisor)
2.	______________________________ Dr. Md. Saifur Rahman Professor and Head Department of Electrical and Electronic Engineering (EEE) Bangladesh University of Engineering and Technology (BUET) Dhaka-1000, Bangladesh	Member (Ex-Officio)
3.	______________________________ Dr. Md. Shah Alam Associate Professor Department of Electrical and Electronic Engineering (EEE) Bangladesh University of Engineering and Technology (BUET) Dhaka-1000, Bangladesh	Member
4.	______________________________ Dr. A. B. M. Siddique Hossain Professor and Dean Faculty of Engineering American International University-Bangladesh	Member (External)

Dedicated to

My beloved parents

And

Honorable teachers,

Who brought me to this enlightened stage of life

ACKNOWLEDGEMENT

First and foremost, all praises and gratitude to almighty God, who created this mysterious universe and led us in the quest for knowledge.

I would like to express my heartful gratitude and profound respect to my supervisor, Dr. Md. Abdul Matin, Professor, Department of Electrical and Electronic Engineering, Bangladesh University of Engineering and Technology, Dhaka, Bangladesh, for his continuous guidance, support and invaluable advice throughout the progress of my research work for the last two years.

I also like to thank my colleagues and superiors who give me the opportunity to finish this thesis work. I also acknowledge the valuable support provided by my cordial friend Md. Gaffar in this regard.

Last, but not the least, I would like to convey my deepest gratitude to my parents, whose contributions are inherent in every word of this work.

ABSTRACT

A compact elliptical-function lowpass filter using modified stepped impedance resonator is designed in this thesis. This is done by introducing two triangular coupled structures inside the filter proposed by Kai Chang in 2003. The model is evaluated with MoM simulation with good agreement. The proposed filter vastly improves the performance of the filter. The additional triangular structure suppresses the harmonic by adding poles at harmonic frequency. The filter is modeled using first order transmission line model as an equivalent L-C network. The equivalent circuit proposed here also can give the cutoff frequency, rejection rate, and stopband rejection within ±5% error range. The filter is fabricated on a 0.254mm thick RT/Duroid 5880 substrate with a relative dielectric constant ε_r=2.2. For single proposed filter, the return loss is better than 17 dB from DC to 1.488 GHz where the insertion loss is less than 0.13 dB. The rejection is greater than -14 dB from 2.0 GHz to 13 GHz. The proposed filter is about 30% smaller than the filter proposed by Kai Chang in 2003 for same cut-off frequency. In this thesis the proposed filter is modeled up to 5GHz lowpass response. By cascading these lowpass filters with different length and width, having different 3dB cut-offs, more rejection in stopband can be obtained to design efficient filter for practical wireless communication systems.

TABLE OF CONTENTS

LIST OF TABLES

LIST OF FIGURES

LIST OF ABBREVIATIONS

RF	:	Radio frequency
SIR	:	Stepped Impedance Resonator
FEM	:	Finite Element Method
MEMS	:	Micro electro mechanic system
MMIC	:	Monolithic microwave integrated circuit
MoM	:	Method of Moment
TEM	:	Transverse Electro Magnetic
RFID	:	Radio frequency identification
ADS	:	Advanced Design System
CAD	:	Computer aided design

LIST OF SYMBOLS

Z_c,	:	Characteristic impedance
Z_0	:	Intrinsic impedance
S	:	Scattering parameter
S_{11}, S_{22}	:	Reflection coefficient
S_{12}, S_{21}	:	Transmission coefficient
L_A	:	Insertion loss
L_R	:	Return loss
Ω	:	Frequency variable
n	:	Order of filter
η	:	Wave impedance in free space
ε	:	Permittivity
ε_0	:	Vacuum permittivity (8.854×10^{-12} Fm^{-1})
ε_r	:	Relative dielectric constant
μ	:	Permeability
ε_{re}	:	Effective dielectric constant
C_a	:	Capacitance per unit length with the dielectric substrate replaced by air
C_d	:	Capacitance per unit length with the dielectric substrate
c	:	Velocity of electromagnetic waves in free space (c =3.0 × 10^8 m/s)
t	:	Strip line thickness
W	:	Microstrip width
h	:	Height of the substrate
θ_o	:	Odd mode electrical length of the lines
θ_e	:	Even mode electrical length of the lines
Z_{0o}	:	Odd mode characteristic impedance
Z_{0e}	:	Even mode characteristic impedance
C_{odd}	:	Odd capacitance
C_{even}	:	Even capacitance
Z_o	:	Odd impedance
Z_e	:	Even impedance

λ_g	:	Given wavelength of quasi-TEM mode
λ_0	:	Free space wavelength
γ	:	Complex propagation constant
α	:	Attenuation constant
β	:	Propagation constant
β_s	:	Phase constant
ω	:	Angular frequency
ε_0	:	Vacuum permittivity
C_{ga}	:	Fringe capacitances for the air
C_{gd}	:	Fringe capacitances for the dielectric regions
C_{Δ}	:	Capacitance due to junction discontinuity
C_f	:	Fringe capacitance
C_p	:	Parallel plate capacitance

CHAPTER 1

INTRODUCTION

1.1 Introduction

Recent advances in modern wide-band radar and wireless communication applications demand high performance, low cost and compact RF subsystem. Therefore, much attention has been devoted for compact microwave devices. Microwave filters are the basic building blocks with frequency-selective or filtering functionality in the development of various wireless systems that operate at frequency ranges above 300 MHz. Filters block play a key role in effectively transmitting the desired signals in certain pass-band regions while attenuating all the undesired signals in the remaining band-stop regions.

Filters play important roles in many RF/microwave applications. They are used to separate or combine different frequencies. The electromagnetic spectrum is limited and has to be shared; filters are used to select or confine the RF/microwave signals within assigned spectral limits. Emerging applications such as wireless communications continue to challenge RF/microwave filters with ever more stringent requirements—higher performance, smaller size, lighter weight, and lower cost. Depending on the requirements and specifications, RF/microwave filters may be designed as lumped element or distributed element circuits; they may be realized in various transmission line structures, such as waveguide, coaxial line, and microstrip. The recent advance of novel materials and fabrication technologies, including monolithic microwave integrated circuit (MMIC), micro electro mechanic system (MEMS), micromachining, high-temperature superconductor (HTS), and low-temperature cofired ceramics (LTCC), has stimulated the rapid development of new microstrip and other filters. In the meantime, advances in computer-aided design (CAD) tools such as full-wave electromagnetic (EM) simulators have revolutionized filter design. The development of efficient methods for tuning both the center frequency and bandwidth of the filter response should be one of the main goals of filter designing. Tunable-bandwidth microwave filters are especially useful for the design of high-frequency multifunction receivers supporting multiple information signals with different frequency-bands

1.2 Related Works and Scope

Microstrip filters are of considerable research interest in recent years. In the last decade, it become more important for wireless and stacked semiconductor network. In all the electrical system and communication, wireless system is becoming more and more popular. To fulfill the requirement of the demand, the amount of research work on wireless system is more than ever. Small size lowpass filters are frequently required in many communication systems to suppress harmonics and spurious signals. As the devices become smaller, the field of microstip antenna and filter is getting bigger. Research has been done on different types of microtrip filters over the last few decades. Among them are the stepped-impedance filters, open-stub filters, semi-lumped element filters, parallel-coupled half wavelength resonator filters, hairpin-line filters, inter-digital and combline filters, pseudo-combline filters, stub-line filters.

However, elliptic-function Stepped Impedance Resonator (SIR) has been studied for a long time as both lowpass filter and bandpass filter. Hsieh et. al. [1] first proposed compact inverted ‘U’ shaped Stepped Impedance Resonator. They modeled the filter by transmission line circuit design and verified by Hybrid Finite Element Method (FEM) and Method of Moment (MoM) simulator. The IE3D simulator was used by them. It showed good matches to the experimental data. The problem for this proposed filter is that, it does not have a wide stopband. To achieve wide stopband they proposed to cascade the filter. But cascading those filter increases the size of the filter. The reason of using elliptic-function Stepped Impedance Resonator over the Butterworth and Chebyshev is to have sharp cut-off frequency response. To achieve similar sharp cut-off Butterworth and Chebyshev filters need to be cascaded. But increasing the number of sections also increases the size of the filter and insertion loss.

A number of publications have followed on designs to suppress higher unwanted modes. They have used different techniques to suppress the higher harmonic modes, also known as spurious modes. J. H. Cho et. al. [2] proposed a new approach using an aperture. They used an aperture on the backside of the substrate. This eliminates the parasitic capacitance of the single transmission line. C. L. Huang et. al. [3] have used high permittivity substrate to increase the bandwidth suppressing the spurious modes.

They used high permittivity ceramic material with high quality factor. They cascaded their proposed filter to have a bandpass response. In 2007 Y. W. Chen et. al.[4] proposed a bandpass filter design using two connected quarter-wavelength SIRs with the joint shorting to the ground. It was built by a three-sectioned SIR of half-wavelength with its middle point shorting to ground through a metallic via hole. M.H. Yang et. Al [5] also proposed a new structure for broad stopband lowpass filter.

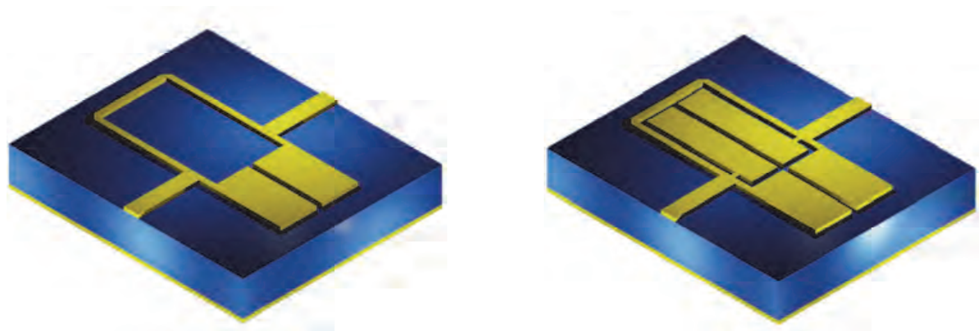

(a) (b)

Figure 1.1 Microstrip SIR hairpin filter proposed by (a) Hsieh et. al. [1]
(b) M.H. Yang et. Al [5]

Simultaneously, compactness of the filter becomes more important now-a-days. Presently, Monolithic Microwave Integrated Circuit (MMIC) and small dimension device operation become evident in small structure filters. Cheng-Hsing Hsu et. al.[6] designed a four-pole elliptical function band-pass filter using miniaturized microstrip inter-digital structure and step-impedance structure having parallel coupled lines.

By studying more recent works of M. Sagawa et. al.'s [7] and Kuo-Sheng Chin et. al.[8] work, it is convenient to design a novel microstrip filter which would suppress spurious modes and is compact in size. The design includes both the circuit modeling of the proposed filter and its verification by hybrid FEM/MoM simulator.

1.3 Objectives

The main objectives of this thesis are:

i. To design an elliptic-function microstrip lowpass filter using inverted 'U' resonator. This model will be verified using Full-Wave EM Simulator. A 3D

Finite Element Method (FEM) / Method of Moment (MoM) simulation with accurate meshing should approximate the practical filter realization [10]-[11].

ii. To derive the equivalent circuit for the proposed filter and verify the results.

iii. To improve the frequency response of the filter by some structural modification performed on the previously designed lowpass filters. This structural modification will relate the equivalent circuit model in such a manner that if the width of the metal strips changes, the capacitance between metal and ground will increase.

iv. Suppression of the spurious effect (higher harmonic modes) of this lowpass filter will be done.

v. To make the stopband region of this filter broad.

vi. To achieve attainable compactness with respect to its previous designs for RFID, MMIC application.

1.4 Organization of the Thesis

Following this introduction, Chapter 2 provides a review of various concepts of micorstrip filters, transmission line models and different types of filters. This chapter covers the essential theories required for the design of the proposed filter.

In chapter 3, a new stepped impedance resonator filter model is proposed and its equivalent circuit is presented. The mathematical model of the equivalent circuit's parameters is derived in this chapter.

In Chapter 4, the frequency response of proposed structures and its variants are discussed on the basis of the computer simulation using Agilent Advanced Design System (ADS) 2011.01.

In Chapter 5, the performance of the equivalent circuit is evaluated. Equivalent circuit for some different filter is derived and their performance is compared.

Chapter 6 focuses on the major findings and improvements of this thesis. The result found from layout simulation is compared with the result found from proposed equivalent circuit.

Lastly, a brief summary of the contributions regarding the presented work and suggestion for future research work conclude the thesis.

CHAPTER 2

THEORY

2.1 Introduction

This chapter covers some essential theory to understand the filter and equivalent circuit proposed in this thesis. Among them are network analysis, scattering parameters, ABCD parameters, different types of filter responses, microstrip structures and the effect of discontinuity in microstrip structure etc. These are discussed in brief and only the essential parts needed for understanding this thesis are explained.

2.2 Network Analysis

Microstrip filters can be represented as a two port network shown on Figure 2.1, where V_1, V_2 and I_1, I_2 are the voltage and current variables at the port 1 and port 2, respectively, Z_{01} and Z_{02} are intrinsic impedance, and E_s is the source voltage.

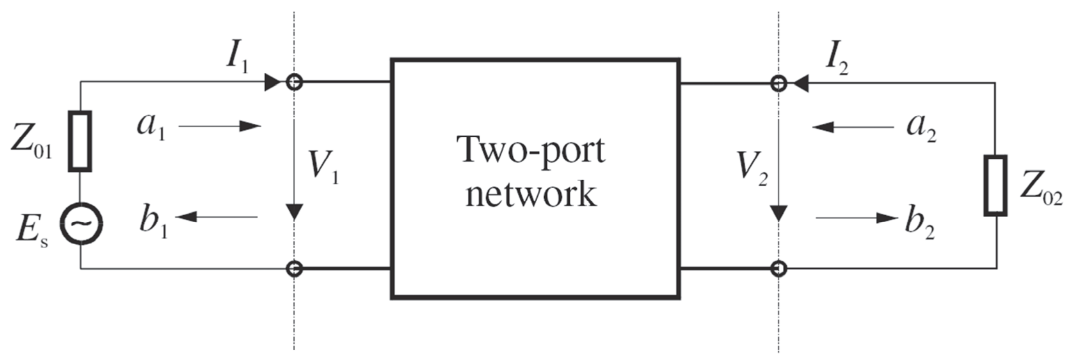

Figure 2.1 Two-port network showing network variables

As the measuring of the voltage and current at microwave frequencies are very difficult, wave variables a_1, a_2, b_1, b_2 are introduced where a indicating the incident waves and b the reflected waves. These wave variables has an unique relationship as shown,

$$V_n = \sqrt{Z_{on}}\left(a_n + b_n\right) \tag{2.1}$$

n=1 and 2

$$I_n = \frac{1}{\sqrt{Z_{on}}}\left(a_n - b_n\right) \tag{2.2}$$

$$a_n = \frac{1}{2}\left(\frac{V_n}{Z_{on}} + \sqrt{Z_{on}}\, I_n\right) \tag{2.3}$$

n=1 and 2

$$b_n = \frac{1}{2}\left(\frac{V_n}{\sqrt{Z_{on}}} - \sqrt{Z_{on}}\, I_n\right) \tag{2.4}$$

The power at port *n* is,

$$P_n = \frac{1}{2}\mathrm{Re}\left(V_n.I^*{}_n\right) = \frac{1}{2}\left(a_n a_n{}^* - b_n b^*{}_n\right) \tag{2.5}$$

2.3 Scattering Parameters

The scattering or *S* parameters of a two-port network are defined in terms of the wave variables as [9],

$$S_{11} = \left.\frac{b_1}{a_1}\right|_{a_2=0} \quad S_{12} = \left.\frac{b_1}{a_2}\right|_{a_1=0}$$

$$S_{21} = \left.\frac{b_2}{a_1}\right|_{a_2=0} \quad S_{22} = \left.\frac{b_2}{a_2}\right|_{a_1=0}$$

Where $a_n = 0$ implies a perfect impedance match. So it can be written as following,

$$\begin{bmatrix} b_1 \\ b_2 \end{bmatrix} = \begin{bmatrix} S_{11} & S_{12} \\ S_{21} & S_{22} \end{bmatrix} . \begin{bmatrix} a_1 \\ a_2 \end{bmatrix}$$

Where, the matrix containing the *S* parameters is referred to as the scattering matrix or *S* matrix, which may simply be denoted by *[S]*.

Here S_{11} and S_{22} are called reflection coefficient, whereas S_{12} and S_{21} are called transmission coefficient. These are the parameters directly measurable at microwave frequencies. In dB, S_{11} and S_{12} are called return loss and insertion loss respectively.

Insertion loss,

$$L_A = -20\log\left|S_{mn}\right| dB \text{ m, n =1,2} \quad (\text{m} \neq \text{n}) \tag{2.6}$$

And return loss,

$$L_R = 20\log\left|S_{nn}\right| dB \quad \text{n=1,2} \tag{2.7}$$

2.4 ABCD Parameters

The *ABCD* parameters of a two-port network are given by,

$$A = \frac{V_1}{V_2}\bigg|_{I_2=0} \quad B = \frac{V_1}{-I_2}\bigg|_{V_2=0}$$

$$C = \frac{I_1}{V_2}\bigg|_{I_2=0} \quad D = \frac{I_1}{-I_2}\bigg|_{V_2=0}$$

These parameters are actually defined in a set of linear equations in matrix notation,

$$\begin{bmatrix} V_1 \\ I_1 \end{bmatrix} = \begin{bmatrix} A & B \\ C & D \end{bmatrix} \cdot \begin{bmatrix} V_2 \\ -I_2 \end{bmatrix}$$

Where, the matrix comprised of the *ABCD* parameters is called the *ABCD* matrix. Sometimes, it may also be referred to as the transfer or chain matrix. The *ABCD* parameters have the following properties,

$AD – BC = 1$, for a reciprocal network
$A = D$, for a symmetrical network

If the network is lossless, then *A* and *D* will be purely real and *B* and *C* will be purely imaginary.

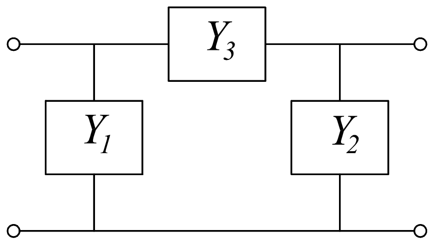

$$A = 1 + \frac{Y_2}{Y_3} \qquad B = \frac{1}{Y_3}$$

$$C = Y_1 + Y_2 + \frac{Y_1 Y_2}{Y_3} \qquad D = 1 + \frac{Y_1}{Y_3}$$

(a)

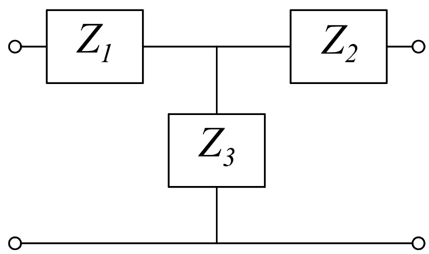

$$A = 1 + \frac{Z_1}{Z_3} \qquad B = Z_1 + Z_2 + \frac{Z_1 Z_2}{Z_3}$$

$$C = \frac{1}{Z_3} \qquad D = 1 + \frac{Z_2}{Z_3}$$

(b)

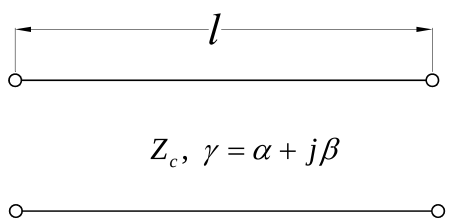

$$A = \cosh \gamma l \qquad B = Z_c \sinh \gamma l$$

$$C = \frac{\sinh \gamma l}{Z_c} \qquad D = \cosh \gamma l$$

(c)

Figure 2.2 Two-port networks and their ABCD parameters (a) π-network (b) T-network (c) Transmission line

2.5 Basic Concept of Filter

The transfer function of a two-port filter network is a mathematical description of network response characteristics, S_{21}. It can be defined as,

$$\left|S_{21}(j\Omega)\right|^2 = \frac{1}{1 + \varepsilon^2 F_n^2(\Omega)} \tag{2.8}$$

Where ε is the ripple constant, $F_n(\Omega)$ represents a filtering or characteristic function and Ω is a frequency variable. it is convenient to let Ω represent a radian frequency variable of a lowpass prototype filter that has a cutoff frequency at $\Omega=\Omega_c$ for Ω_c = 1 (rad/s). For linear network, the transfer function can be defined as a rational function,

$$S_{21}(p) = \frac{N(p)}{D(p)}$$

N(p) and *D(p)* are numerator and denominator polynomials. The roots of *N(p)* is called zeros and the roots of *D(p)* is called poles. At pole, $S_{21}(\Omega)$ becomes higher, i.e 0dB.

Now, insertion loss $L_A = 10\log\frac{1}{\left|S_{21}(j\Omega)\right|^2}$ (dB)

$$\text{Now, } L_A = 10\log\frac{D^2(p)}{N^2(p)} \quad \text{(dB)} \tag{2.9}$$

$$= 10\log\left|\frac{D(p)}{N(p)}\right|^2 \quad \text{(dB)}$$

So, pole of S_{21} becomes the zeroes of L_A (undefined value in dB)and zero of S_{21} becomes the poles of L_A (0 in dB).

Since $\left|S_{11}\right|^2 + \left|S_{21}\right|^2 = 1$, for a lossless passive, two port network, the return loss response of the filter can be found, $L_R = 10\log[1 - \left|S_{21}(j\Omega)\right|^2]$ (dB)

Poles and zeroes for L_R can be shown as the opposite vision of the previous words for insertion loss.

As $S_{12}(\Omega)$ is a rational function so, *N(p)* and *D(p)* will be factors of zeroes and poles. To have a stable response, we need all the poles of S_{21} to be in the left plane of pole-zero plane (real-imaginary axis). Here *D(p)*'s root should be in the left plane where *N(p)*'s root can be anywhere on the pole-zero plane. The roots of *N(p)* is called transmission zero. But the position of pole may change the characteristics of filter.

2.5.1 Butterworth response

The amplitude-squared transfer function for Butterworth filters that have an insertion loss L_{Ar}= 3.0 dB at the cutoff frequency Ω_c= 1 is given by,

$$\left|S_{21}(j\Omega)\right|^2 = \frac{1}{1+\Omega^{2n}} \tag{2.10}$$

Where n is the degree or the order of filter, which corresponds to the number of reactive elements, required in the lowpass prototype filter. This type of response is also referred to as maximally flat because its amplitude-squared transfer function defined in (2.10) has the maximum number of ($2n$ – 1) zero derivatives at Ω= 0.Therefore, the maximally flat approximation to the ideal lowpass filter in the passband is best at Ω= 0, but deteriorates as Ω approaches the cutoff frequency Ω_c. Figure 2.3 shows a typical maximally flat response.

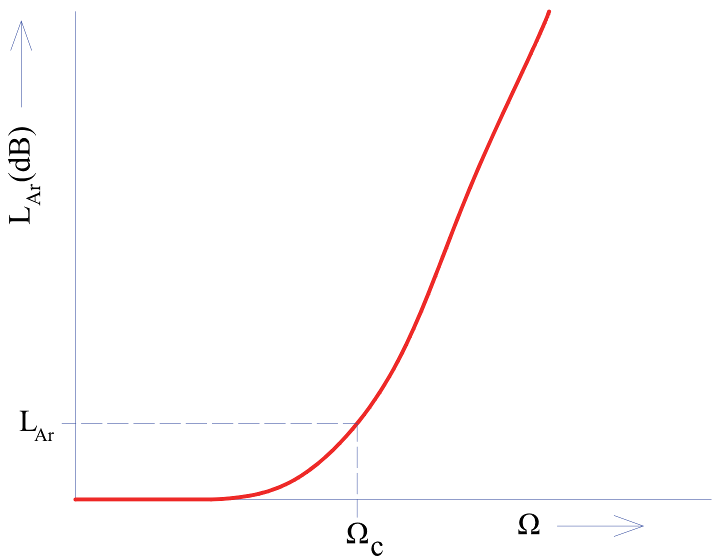

Figure 2.3 Butterworth (maximally flat) lowpass response

A rational transfer function constructed from (2.10) is [12–13]

$$S_{21}(p) = \frac{1}{\prod_{i=1}^{n}(p - p_i)} \tag{2.11}$$

With,

$$p_i = j \exp\left[\frac{(2i-1)\pi}{2n}\right] \tag{2.12}$$

There is no finite-frequency transmission zero .all the zeros of $S_{21}(p)$ are at infinity and the poles p_i lie on the unit circle in the left half-plane at equal angular spacing, since $|p_i|$ = 1 and Arg p_i= $(2i – 1)\pi/2n$. This is illustrated in Figure 2.4.

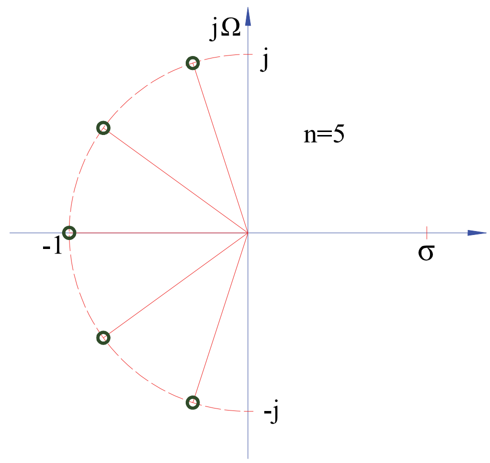

Figure 2.4 Pole distribution for Butterworth (maximally flat) response

2.5.2 Chebyshev response

The Chebyshev response that exhibits the equal-ripple passband and maximally flat stopband is shown in Figure 2.5. It is defined as,

$$\left|S_{21}(j\Omega)\right|^2 = \frac{1}{1+\varepsilon^2 T_n^2(\Omega)} \tag{2.13}$$

where the ripple constant ε is related to a given passband ripple L_{Ar} in dB by,

$$\varepsilon = \sqrt{10^{\frac{L_{Ar}}{10}} - 1} \tag{2.14}$$

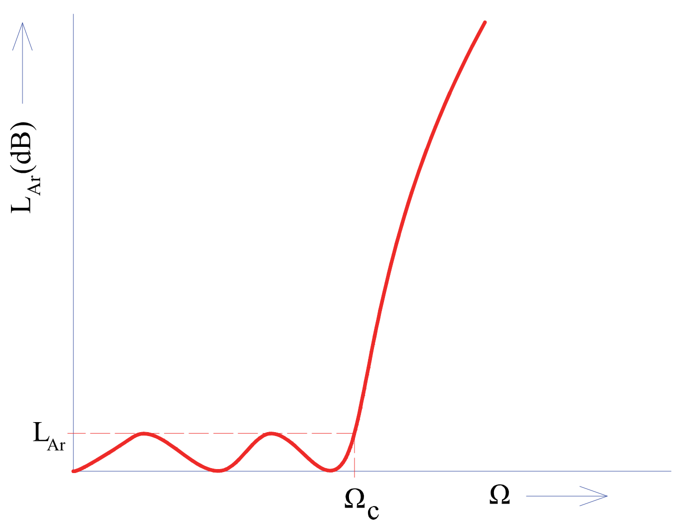

Figure 2.5 Chebyshev lowpass response

$T_n(\Omega)$ is a Chebyshev function of the first kind of order n, which is defined as

$$T_n(\Omega) = \begin{cases} \cos\left(n\cos^{-1}\Omega\right) & \text{for } |\Omega| \le 1 \\ \cosh\left(n\cosh^{-1}\Omega\right) & \text{for } |\Omega| \ge 1 \end{cases} \tag{2.15}$$

Hence, the filters realized from (2.13) are commonly known as Chebyshev filters. Rhodes [13] has derived a general formula of the rational transfer function from (2.15) for the Chebyshev filter, that is,

$$S_{21}(p) = \frac{\prod_{i=1}^{n}\left[\eta^2 + \sin^2(i\pi/n)\right]^{1/2}}{\prod_{i=1}^{n}(p + p_i)} \tag{2.16}$$

With,

$$p_i = j\cos\left[\sin^{-1} j\eta + \frac{(2i-1)\pi}{2n}\right] \tag{2.17}$$

$$\eta = \sinh\left(\frac{1}{n}\sinh^{-1}\frac{1}{\varepsilon}\right) \tag{2.18}$$

Similar to the maximally flat case, all the transmission zeros of $S_{21}(p)$ are located at infinity. Therefore, the Butterworth and Chebyshev filters dealt with so far are sometimes referred to as all-pole filters. However, the pole locations for the Chebyshev case are different, and lie on an ellipse in the left half-plane. The major axis of the ellipse is on the $j\Omega$-axis and its size is $\sqrt{1+\eta^2}$; the minor axis is on the σ-axis and is of the size η. The pole distribution is shown in Figure 2.6 for n = 5.

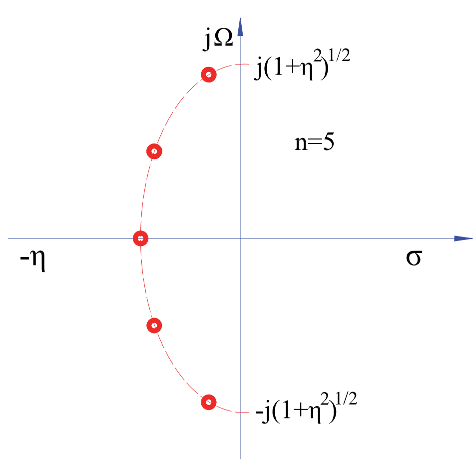

Figure 2.6 Pole distribution for a Chebyshev response for *n*=5

2.5.3 Elliptical function response

The response that is equal-ripple in both the passband and stopband is the elliptic function response, as illustrated in Figure 2.7. The transfer function for this type of response is,

$$\left|S_{21}\left(j\Omega\right)\right|^2 = \frac{1}{1+\varepsilon^2 F_n^2\left(\Omega\right)} \tag{2.19}$$

Where,

$$F_n(\Omega) = \begin{cases} M \dfrac{\prod_{i=1}^{n/2}(\Omega_i^2 - \Omega^2)}{\prod_{i=1}^{n/2}(\Omega_s^2/\Omega_i^2 - \Omega^2)} & \text{for } n \text{ even} \\ N \dfrac{\prod_{i=1}^{(n-1)/2}(\Omega_i^2 - \Omega^2)}{\prod_{i=1}^{(n-1)/2}(\Omega_s^2/\Omega_i^2 - \Omega^2)} & \text{for } n (\geq 3) \text{ odd} \end{cases} \tag{2.20}$$

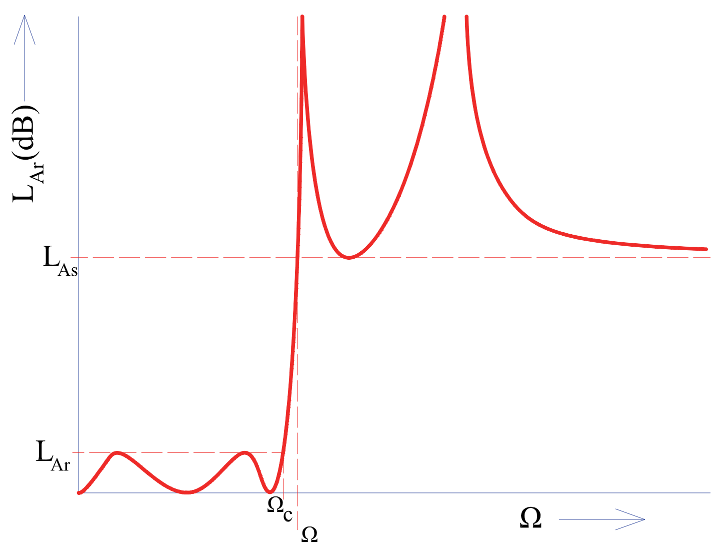

Figure 2.7 Elliptic function lowpass response

Where Ω_i $(0<\Omega_i<1)$ and $\Omega_s>1$ represents some critical frequencies. M and N are constants to be defined [14-15]. $F_n(\Omega)$ will oscillate between ±1 for $|\Omega| \leq 1$, and $|F_n(\Omega = \pm 1)| = 1$.

2.6 Microstrip Structure

A conduction strip with a width W is shown in Figure 2.8. It has a thickness t and is on the top of a dielectric substrate that has a relative dielectric constant ε_r and a thickness h. There is ground plane at the bottom.

The fields in the microstrip extend within two media, air above and dielectric below. So the structure is inhomogeneous. Due to this inhomogeneous nature, it does not support pure TEM wave inside the substrate. This is because, a pure TEM wave has only transverse components, and its propagation velocity depends only on the material properties, namely the permittivity ε and the permeability μ. However, with the presence of the two guided-wave media (the dielectric substrate and the air), the waves in a microstrip line will have no vanished longitudinal components of electric and magnetic fields, and their propagation velocities will depend not only on the material properties, but also on the physical dimensions of the microstrip. It can be approximated by quasi-TEM approximation. The phase velocity entirely depends on the material properties and the dimension of the microstrip. For quasi-TEM wave we neglect the longitudinal wave where transverse wave has greater value. So the transverse field approximates the pure TEM which is called quasi-TEM wave.

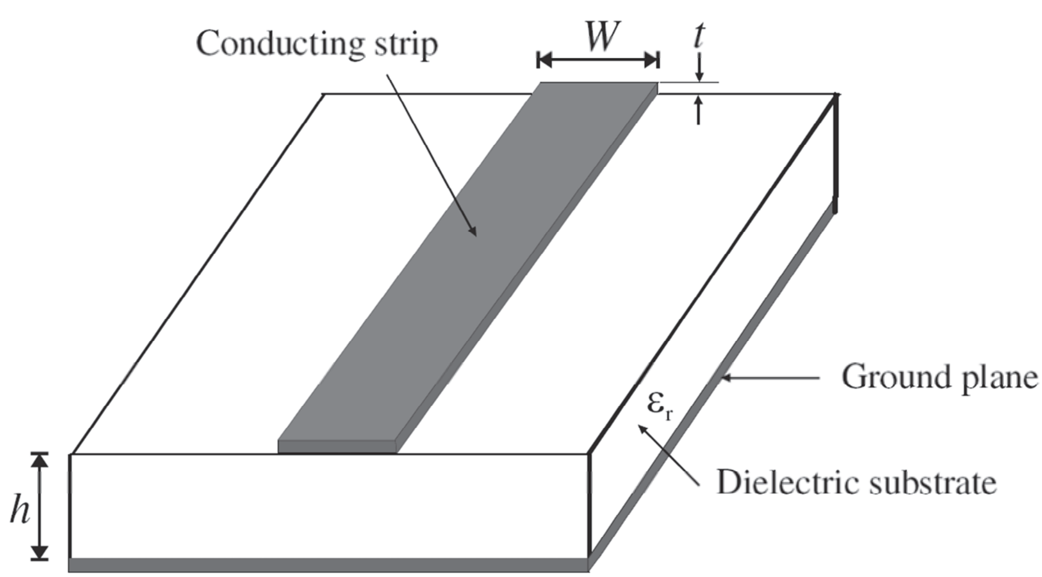

Figure 2.8 General microstrip structure

2.7 Effective Dielectric Constant and Characteristic Impedance

In the quasi-TEM approximation, a homogeneous dielectric material with an effective dielectric permittivity replaces the inhomogeneous dielectric–air media of microstrip. Transmission characteristics of microstrips are described by two parameters, namely, the effective dielectric constant ε_{re} and characteristic impedance Z_c, which may then be obtained by quasistatic analysis [16]. In quasi-static analysis, the fundamental mode of wave propagation in a microstrip is assumed to be pure TEM. The above two parameters of microstrips are then determined from the values of two capacitances as follows,

$$\varepsilon_{re} = \frac{C_d}{C_a} \tag{2.21}$$

$$Z_c = \frac{1}{c\sqrt{C_a C_d}} \tag{2.22}$$

in which C_d is the capacitance per unit length with the dielectric substrate present, C_a is the capacitance per unit length with the dielectric substrate replaced by air, and c is the velocity of electromagnetic waves in free space (c =3.0 × 10^8 m/s).

For very thin conductors (i.e., $t \rightarrow 0$), the closed-form expressions that provide accuracy better than one percent are given [17] as follows,

For $\frac{W}{h} \leq 1$:

$$\varepsilon_{re} = \frac{\varepsilon_r + 1}{2} + \frac{\varepsilon_r - 1}{2}\left\{\left(1 + 12\frac{h}{W}\right)^{-\frac{1}{2}} + 0.04\left(1 - \frac{W}{h}\right)^2\right\} \tag{2.23}$$

$$Z_c = \frac{\eta}{2\pi\sqrt{\varepsilon_{re}}} \ln\left(\frac{8h}{W} + 0.25\frac{W}{h}\right) \tag{2.24}$$

For $\frac{W}{h} \geq 1$:

$$\varepsilon_{re} = \frac{\varepsilon_r + 1}{2} + \frac{\varepsilon_r - 1}{2}\left(1 + 12\frac{h}{W}\right)^{-\frac{1}{2}} \tag{2.25}$$

$$Z_c = \frac{\eta}{\sqrt{\varepsilon_{re}}}\left\{\frac{W}{h} + 1.393 + 0.677\ln\left(\frac{W}{h} + 1.444\right)\right\}^{-1} \tag{2.26}$$

Where, η=120π ohms is the wave impedance in free space.

W=strip width

h=height of the substrate

A more accurate model for ε_{re} proposed by Hammerstad and Jensen [18] .Which is,

$$\varepsilon_{re} = \frac{\varepsilon_r + 1}{2} + \frac{\varepsilon_r - 1}{2}\left(1 + \frac{10}{u}\right)^{-ab} \tag{2.27}$$

Where, u=W/h and

$$a = 1 + \frac{1}{49}\ln\left(\frac{u^4 + \left(\frac{u}{52}\right)^2}{u^4 + 0.432}\right) + \frac{1}{18.7}\ln\left[1 + \left(\frac{u}{18.1}\right)^3\right] \tag{2.28}$$

$$b = 0.564\left(\frac{\varepsilon_r - 0.9}{\varepsilon_r + 3}\right)^{0.053} \tag{2.29}$$

The accuracy of this model is better than 0.2% for $\varepsilon_r \leq 128$ and $0.01 \leq u \leq 100$.

2.8 Hairpin Filters

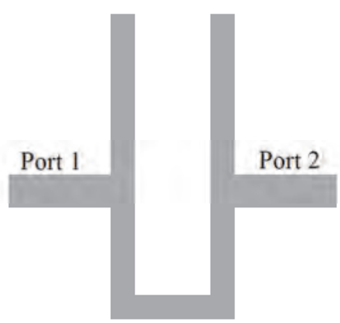

Figure 2.9 Hairpin filter structure

Hairpin-line filters are compact structures. They may conceptually be obtained by folding the resonators of parallel-coupled, half-wavelength resonator filters into a “U” shape. This type of “U” shaped (Figure 2.9) resonator is called hairpin resonator [9].

The advantages of the hairpin resonator are,

1) It is compact because of folding the resonators of parallel-coupled, half-wavelength resonator filters to reduce the length of the couple line.
2) Better coupling because of two parallel line coupling of adjacent U-shape resonators.

2.9 Coupled Line Transmission Line

The system of two parallel coupled lines is shown in Figure 2.10. Now, if the port 3 and port 4 are considered as open, then $I_3=I_4=0$. Then the two port network seems to be [22],

$$\begin{bmatrix} V_1 \\ V_2 \end{bmatrix} = \begin{bmatrix} Z_{11} & Z_{13} \\ Z_{21} & Z_{22} \end{bmatrix} \begin{bmatrix} I_1 \\ I_2 \end{bmatrix}$$

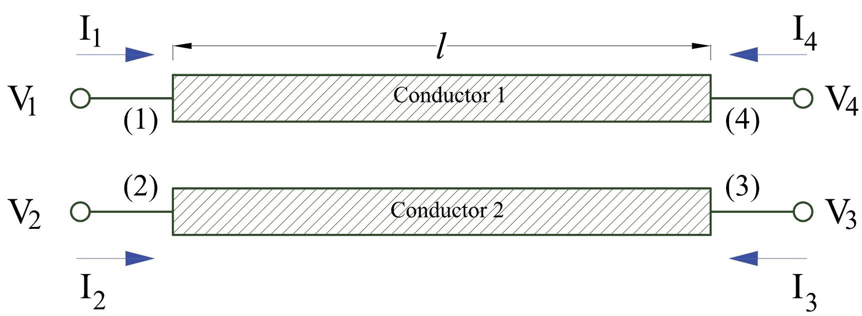

Figure 2.10 Schematic of pair of coupled-lines

Where,

$$\begin{bmatrix} Z_{11} & Z_{13} \\ Z_{21} & Z_{22} \end{bmatrix} = -j\frac{1}{2}\begin{bmatrix} Z_{0e}\cot\theta_e + Z_{0o}\cot\theta_o & Z_{0e}\mathrm{cosec}\,\theta_e - Z_{0o}\mathrm{cosec}\,\theta_o \\ Z_{0e}\mathrm{cosec}\,\theta_e - Z_{0o}\mathrm{cosec}\,\theta_o & Z_{0e}\cot\theta_e + Z_{0o}\cot\theta_o \end{bmatrix}$$

$$= -j\frac{Z_{0e}}{2}\begin{bmatrix} \cot\theta_e & \mathrm{cosec}\,\theta_e \\ \mathrm{cosec}\,\theta_e & \cot\theta_e \end{bmatrix} - j\frac{Z_{0o}}{2}\begin{bmatrix} \cot\theta_o & -\mathrm{cosec}\,\theta_o \\ -\mathrm{cosec}\,\theta_o & \cot\theta_o \end{bmatrix} \quad (2.30)$$

So the Z matrix can be written as,

$$[Z] = -jZ_0\begin{bmatrix} \cot\theta & \mathrm{cosec}\,\theta \\ \mathrm{cosec}\,\theta & \cot\theta \end{bmatrix} \quad (2.31)$$

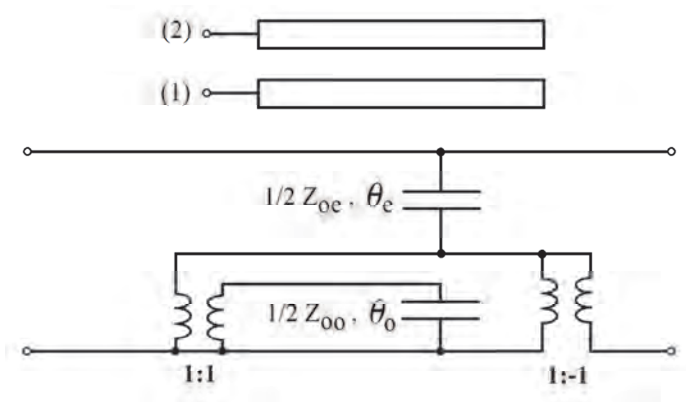

Figure 2.11 Equivalent circuit of a pair comb structured coupled line

Now the ABCD parameter of the above defined transmission line,

$$A = \frac{Z_{0e}\cot\theta_e + Z_{0o}\cot\theta_o}{Z_{0e}\cot\theta_e + Z_{0o}\cot\theta_o} = D$$

$$B = -j\frac{2Z_{0e}Z_{0o}\cot\theta_e\cot\theta_o}{Z_{0e}\cot\theta_e - Z_{0o}\cot\theta_o}$$

$$C = j\frac{2}{Z_{0e}\cot\theta_e - Z_{0o}\cot\theta_o}$$

2.10 Micorstrip Line Step

In microstrip line, when the width of the strip changes abruptly as shown in Figure 2.12, the impedance also changes [19]. The impedance depends on the width of the microstrip line. So by making a step in microstrip line, an impedance step can be created. Step can be of two types, asymmetric and symmetric as shown in Figure 2.13.

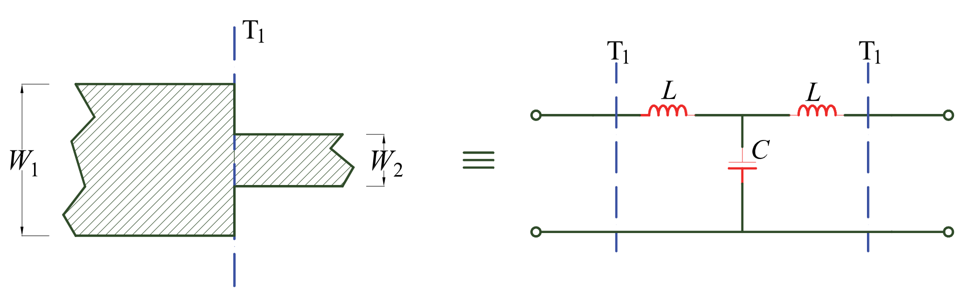

(a) (b)

Figure 2.12 Abrupt change in microstrip line width (a) schematic, (b) equivalent circuit

For $1.5 \le \frac{w_1}{w_2} \le 3.5$ and $\varepsilon_r \le 10.0$,

$$C_s = \sqrt{w_1 w_2}\left[(10.1\log\varepsilon_r + 2.33)\frac{w_1}{w_2} - 12.6\log\varepsilon_r - 3.17\right] \quad \text{(pF/m)} \tag{2.32}$$

For $3.5 \le \frac{w_1}{w_2} \le 10$ and $\varepsilon_r = 9.6$,

$$C_s = \sqrt{w_1 w_2}\left[130.0\log\left(\frac{w_1}{w_2}\right) - 44.0\right] \quad \text{(pF/m)} \tag{2.33}$$

The inductance is calculated with,

$$L_s = h\left[40.5\left(\frac{w_1}{w_2} - 1.0\right) - 75.0\log\left(\frac{w_1}{w_2}\right) + 0.2\left(\frac{w_1}{w_2} - 1.0\right)\right] \quad \text{(nH/m)} \tag{2.34}$$

This equation is accurate within 5.0% for $\frac{w_1}{w_2} \le 5.0$ and $\frac{w_2}{h} = 1.0$

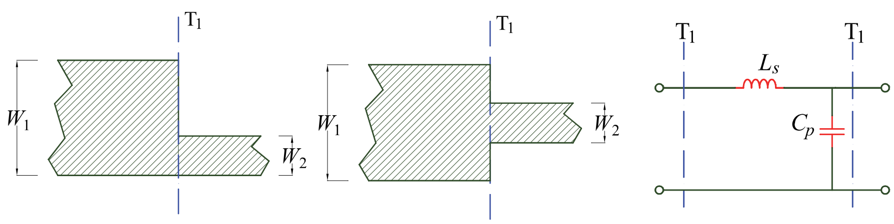

Figure 2.13 Abrupt steps of different type (a)asymmetric (b)symmetric and (c)equivalent circuit

According to Hoffman [20], the parameters of the equivalent circuit shown in Figure 2.13 can be calculated from,

$$L_s = \frac{Z_{L1}}{2.0\pi f}\frac{4.0w_{eff.1}}{\Delta\lambda_1}\left\{\ln\left[\left(\frac{1.0-a^2}{4.0a}\right)\left(\frac{1.0+a}{1.0-a}\right)^{\frac{(a+1/a)}{2}}\right] + 2.0\frac{A+B+2.0D}{AB-D^2} + \left(\frac{w_{eff.1}}{2\Delta\lambda_1}\right)^2\left(\frac{1.0-a}{1.0+a}\right)^{4.0a}\left(\frac{5a^2-1}{1-a^2}+\frac{4a^2D}{3A}\right)^2\right\} \tag{2.35}$$

$$C_p = (0.012 + 0.0039\varepsilon_r)(w_1 - w_2) \quad \text{(pF)} \tag{2.36}$$

Where,

$$A = \left(\frac{1.0+a}{1.0-a}\right)^{2a} \left[\frac{1.0 + \sqrt{1.0 - \left(\frac{2.0 w_{eff.1}}{\Delta \lambda_1}\right)^2}}{1.0 - \sqrt{1.0 - \left(\frac{2.0 w_{eff.1}}{\Delta \lambda_1}\right)^2}} \right] - \frac{1.0 + 3.0a^2}{1.0 - a^2} \tag{2.37}$$

$$B = \left(\frac{1.0+a}{1.0-a}\right)^{a/2} \left[\frac{1.0 + \sqrt{1.0 - \left(\frac{2.0 w_{eff.2}}{\Delta \lambda_2}\right)^2}}{1.0 - \sqrt{1.0 - \left(\frac{2.0 w_{eff.2}}{\Delta \lambda_2}\right)^2}} \right] - \frac{3.0 + a^2}{1.0 - a^2} \tag{2.38}$$

$$D = \left(\frac{4.0a}{1.0 - a^2}\right)^2$$

$$a = \frac{w_{eff.2}}{w_{eff.1}}$$

$$\lambda_n = \frac{c_0}{f\sqrt{\varepsilon_{eff.n}}}$$

$$\Delta = \begin{cases} 1 & \text{for symmetrical steps} \\ 2 & \text{for asymmetrical steps} \end{cases}$$

$$w_{eff.n} = w_n + \frac{w_{eff.static} - w_n}{1.0 + f / f_{p5}}$$

$$w_{eff.static} = \frac{\eta_0 h}{Z_{L0}}$$

Z_{L0} = the impedance of the line calculated with ε_r set to 1.0

$$f_{p5} = \frac{c}{2.0w\sqrt{\varepsilon_r}}.$$

2.11 Microstrip Line Gap

The microstrip gap shown in Figure 2.14 is used in the filters and other circuits as a coupling element. It also occurs as a stray circuit element across surface mount components. According to [21] the equivalent circuit of the line gap can be represented as a transmission line. The capacitance C_a and C_b can be calculated in terms of C_{even} and C_{odd} as followings,

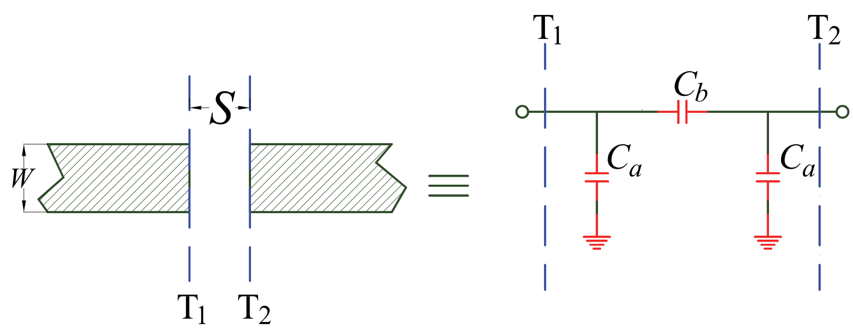

Figure 2.14 Microstrip line gap

$$C_a = \frac{C_{even}}{2} \tag{2.39}$$

and,

$$C_b = \frac{C_{odd}}{2} - \frac{C_{even}}{4} \tag{2.40}$$

where, C_{odd} = odd capacitance

and, C_{even} = even capacitance

CHAPTER 3

MATHEMATICAL DERIVATION

3.1 Introduction

The layout of modified stepped impedance hairpin resonator is showed in Figure 3.1. It has three parts− series line, parallel coupled line and the modified triangular coupled line as shown in Figure 3.2. First the series line has a length of $l_s = l_2 + 2l_3$ and width of w_4. As the length, l_s is much larger than the width w_4, it acts as an inductance. Then the parallel couple line has large width w_3, length l_4 and the gap between the parallel plates, g. The modified triangular couple line has a length, l_6 and a gap between the triangular plates, x . If Z_s is the characteristic impedance of the single transmission line l_s, Z_o and Z_e are the odd and even impedance for the parallel couple line, we took $Z_s > \sqrt{Z_o Z_e}$ to reduce the size of conventional hairpin resonator[1].

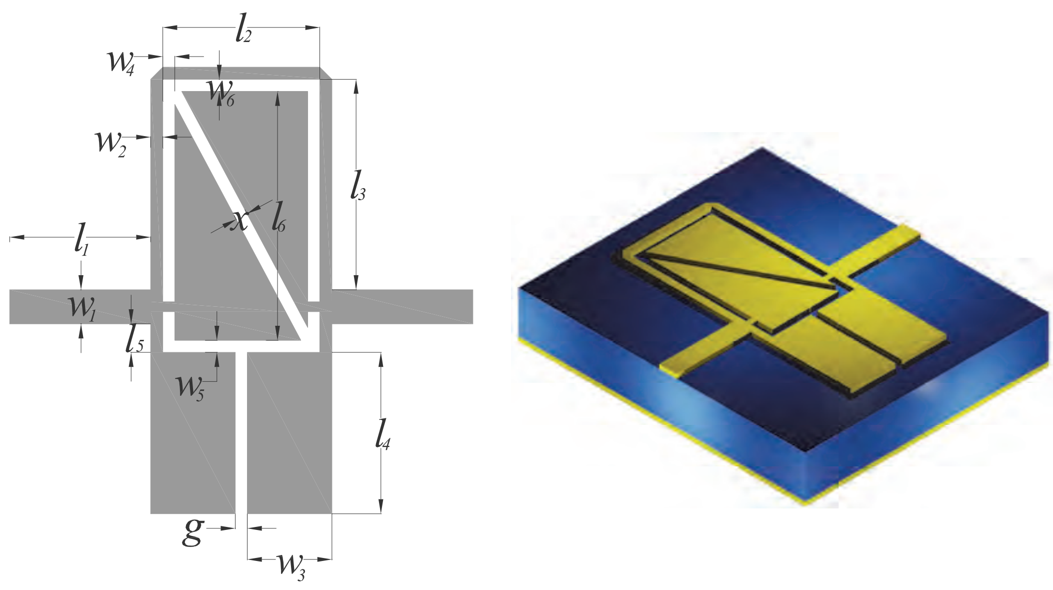

(a) (b)

Figure 3.1 Modified stepped impedance hairpin resonator (a) schematic (b) 3d view

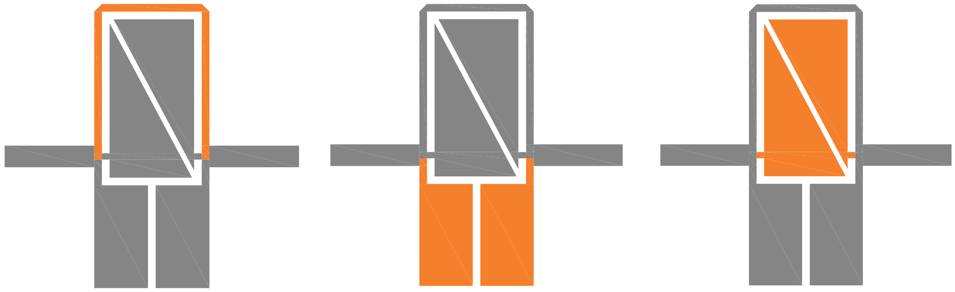

(a) (b) (c)

Figure 3.2 Stepped impedance hairpin resonator highlighting the (a) series line, (b) parallel couple line, (c) modified triangular couple line.

Figure 3.3 shows the Current density of the proposed structure at cut-off frequency. Port 1 is used as input and port 2 is characterized as output port. From Figure 3.3 it is seen that the current density at the series line is very high. So it acts as an inductor. On the other hand parallel coupled line and the modified parallel coupled line has almost zero current density. So it can be assumed that these two act as capacitor.

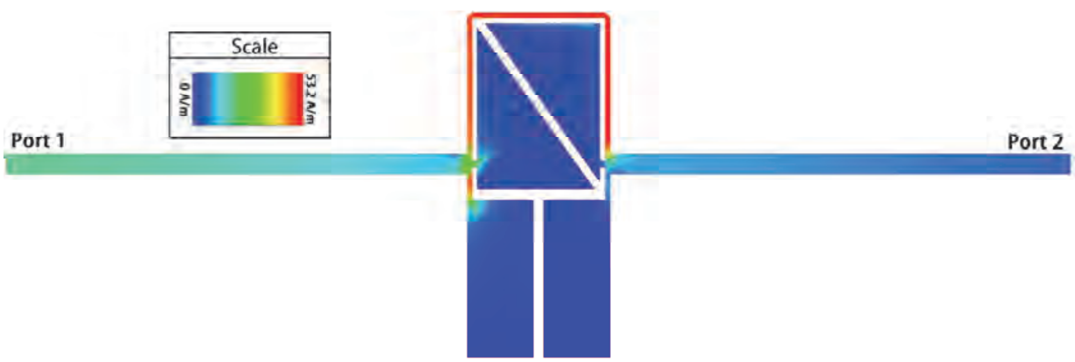

Figure 3.3 Current density of the proposed filter at cut-off frequency

3.2 Series Line

For any single transmission line as we know,

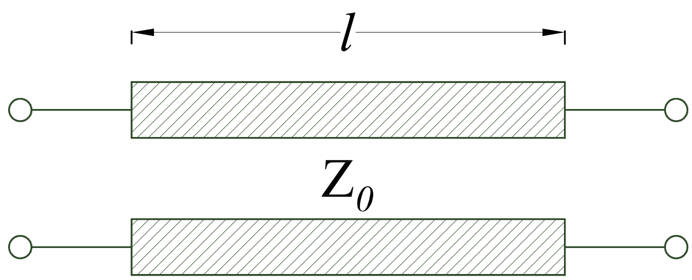

Figure 3.4 Transmission line with a length of *l*

ABCD parameter is described as,

$$\begin{bmatrix} A & B \\ C & D \end{bmatrix} = \begin{bmatrix} \cosh(\gamma l) & Z_0 \sinh(\gamma l) \\ \dfrac{\sinh(\gamma l)}{Z_0} & \cosh(\gamma l) \end{bmatrix} \tag{3.1}$$

For lossless transmission line, $\gamma = \alpha + j\beta$ and $\alpha = 0$. So, $\gamma = j\beta$

So,

$$\begin{bmatrix} A & B \\ C & D \end{bmatrix} = \begin{bmatrix} \cos(\beta l) & jZ_0 \sin(\beta l) \\ \dfrac{j\sin(\beta l)}{Z_0} & \cos(\beta l) \end{bmatrix} \tag{3.2}$$

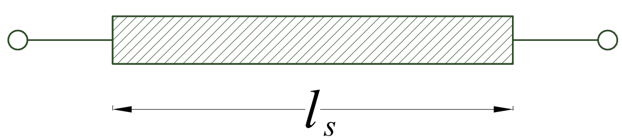

Figure 3.5 series line with a length of l_s

Similarly here, for the series line l_s,

$$\begin{bmatrix} A & B \\ C & D \end{bmatrix} = \begin{bmatrix} \cos(\beta_s l_s) & jZ_s \sin(\beta_s l_s) \\ jY_s \sin(\beta_s l_s) & \cos(\beta_s l_s) \end{bmatrix} \tag{3.3}$$

Where,

β_s= propagation constant

l_s= length of the series line

We can determine β_s as given below,

For $\frac{W}{h} \leq 1$:

$$\varepsilon_{re} = \frac{\varepsilon_r + 1}{2} + \frac{\varepsilon_r - 1}{2}\left\{\left(1 + 12\frac{h}{W}\right)^{-\frac{1}{2}} + 0.04\left(1 - \frac{W}{h}\right)^2\right\} \tag{3.4}$$

$$Z_s = \frac{\eta}{2\pi\sqrt{\varepsilon_{re}}}\ln\left(\frac{8h}{W} + 0.25\frac{W}{h}\right) \tag{3.5}$$

For $\frac{W}{h} \geq 1$:

$$\varepsilon_{re} = \frac{\varepsilon_r + 1}{2} + \frac{\varepsilon_r - 1}{2}\left(1 + 12\frac{h}{W}\right)^{-\frac{1}{2}} \tag{3.6}$$

$$Z_s = \frac{\eta}{\sqrt{\varepsilon_{re}}}\left\{\frac{W}{h} + 1.393 + 0.677\ln\left(\frac{W}{h} + 1.444\right)\right\}^{-1} \tag{3.7}$$

Where,

W= w_s (width of the series line)

η=120π ohms is the wave impedance in free space.

ε_{re}=relative dielectric constant

h=height of the substrate

As the effective dielectric constant has been determined, so the given wavelength of quasi-TEM mode of microstrip is given by,

$$\lambda_g = \frac{\lambda_0}{\sqrt{\varepsilon_{re}}} \tag{3.8}$$

Where, λ_0= free space wavelength.

So the propagation constant,

$$\beta = \frac{2\pi}{\lambda_g} \tag{3.9}$$

Here $\beta = \beta_s$ for series line.

Again, equivalent Pi-model of transmission line of the microstrip (length l_s) is shown as below,

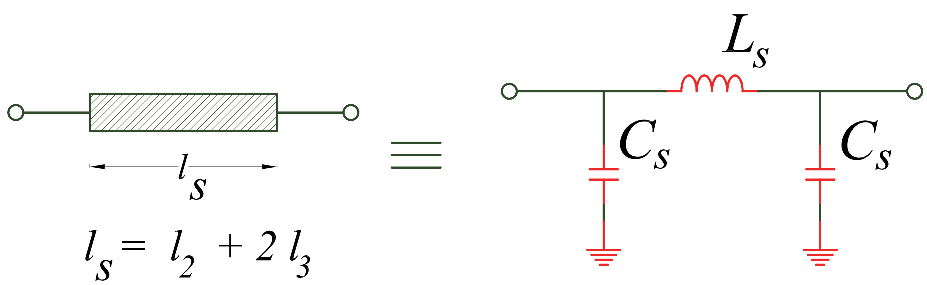

Figure 3.6 Equivalent circuit of a series line

Now the ABCD parameter of the above circuit will be,

$$\begin{bmatrix} A & B \\ C & D \end{bmatrix} = \begin{bmatrix} 1 + Z_L Y_c & Z_L \\ Y_c(2 + Z_L Y_c) & 1 + Z_L Y_c \end{bmatrix} \tag{3.10}$$

Where, $Z_L = j\omega L_s$ and $Y_c = j\omega C_s$.

As the matrix of (3.3) and (3.10) are equivalent, it can be stated that,

$$\begin{bmatrix} \cos(\beta_s l_s) & jZ_s \sin(\beta_s l_s) \\ jY_s \sin(\beta_s l_s) & \cos(\beta_s l_s) \end{bmatrix} = \begin{bmatrix} 1 + Z_L Y_c & Z_L \\ Y_c(2 + Z_L Y_c) & 1 + Z_L Y_c \end{bmatrix} \tag{3.11}$$

Now,

$$jZ_s \sin(\beta_s l_s) = Z_L$$

$$\Rightarrow \qquad j\omega L_s = jZ_s \sin(\beta_s l_s)$$

$$\Rightarrow \qquad L_s = \frac{Z_s \sin(\beta_s l_s)}{\omega} \text{ (H)} \tag{3.12}$$

Again,

$$\cos(\beta_s l_s) = 1 + Z_L Y_c$$

$$\Rightarrow \qquad \cos(\beta_s l_s) = 1 + \left(j\omega L_s\right)\left(j\omega C_s\right)$$

$$\Rightarrow \qquad \cos(\beta_s l_s) = 1 - \omega^2 \times \frac{Z_s \sin(\beta_s l_s) C_s}{\omega}$$

$$\Rightarrow \qquad C_s \omega Z_s \sin(\beta_s l_s) = 1 - \cos(\beta_s l_s)$$

$$\Rightarrow \qquad C_s = \frac{1 - \cos(\beta_s l_s)}{\omega Z_s \sin(\beta_s l_s)} \tag{3.13}$$

3.3 Parallel Couple Line

For the coupled line the structure is given in Figure 3.7.

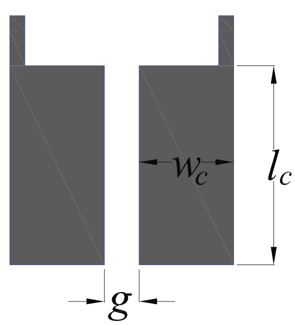

Figure 3.7 Coupled line with line gap *g*

For this stepped impedance resonator, ABCD parameters will be [22],

$$\begin{bmatrix} A & B \\ C & D \end{bmatrix} = \begin{bmatrix} \dfrac{Z_e \cot\theta_e + Z_o \cot\theta_o}{Z_e \cot\theta_e - Z_o \cot\theta_e} & -j\dfrac{2Z_eZ_o \cot\theta_e \cot\theta_o}{Z_e \cot\theta_e - Z_o \cot\theta_o} \\ j\dfrac{2}{Z_e \cot\theta_e - Z_o \cot\theta_o} & \dfrac{Z_e \cot\theta_e + Z_o \cot\theta_o}{Z_e \cot\theta_e - Z_o \cot\theta_e} \end{bmatrix} \quad (3.14)$$

Here $\theta_e = \theta_0$, for a symmetric parallel resonator. So,

$$\begin{bmatrix} A & B \\ C & D \end{bmatrix} = \begin{bmatrix} \dfrac{Z_e + Z_o}{Z_e - Z_o} & -j\dfrac{2Z_eZ_o \cot\theta_e}{Z_e - Z_o} \\ j\dfrac{2}{Z_e \cot\theta_e - Z_o \cot\theta_o} & \dfrac{Z_e + Z_o}{Z_e - Z_o} \end{bmatrix} \quad (3.15)$$

Again for parallel stepped couple line, we can derive an equivalent circuit shown in Figure 3.7.

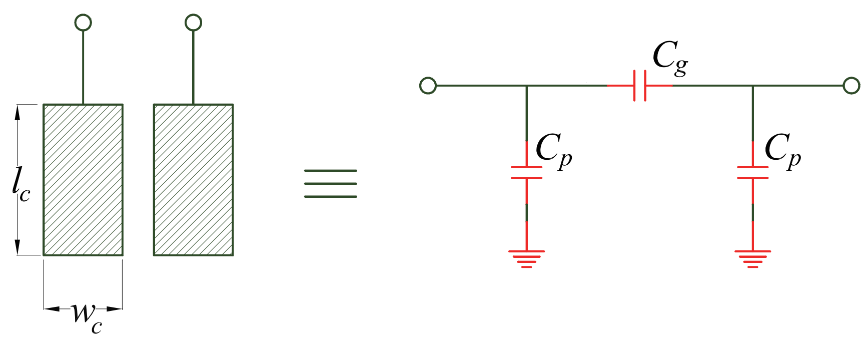

Figure 3.8 Equivalent circuit for coupled line

Now the ABCD parameters of the stepped couple line should be,

$$\begin{bmatrix} A & B \\ C & D \end{bmatrix} = \begin{bmatrix} 1 + Z_gY_p & Z_g \\ Y_p(2 + Z_gY_p) & 1 + Z_gY_p \end{bmatrix} \quad (3.16)$$

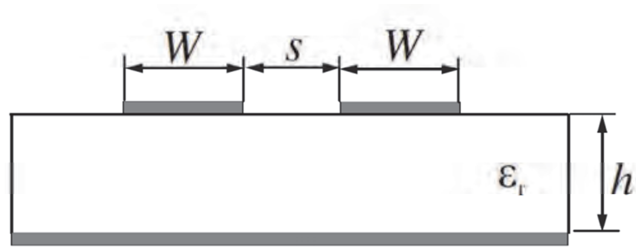

Figure 3.9 Cross section of coupled microstrip line

Here Z_o and Z_e are the parallel couple line's odd and even impedance. For any couple line shown in Figure 3.9, the static electromagnetic field, even and odd impedance can be derived in terms of even and odd capacitance.

$$C_e = C_p + C_f + C'_f \tag{3.17}$$

$$C_o = C_p + C_f + C_{gd} + C_{ga} \tag{3.18}$$

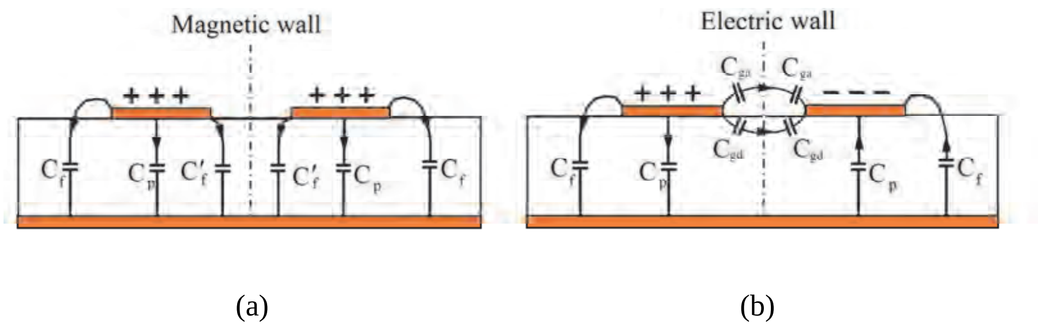

Figure 3.10 Quasi-TEM modes of a pair of coupled microstrip lines for
(a) even mode; (b) odd mode.

In these expressions, C_p denotes the parallel plate capacitance between the strip and the ground plane, and hence is given by,

$$C_p = \varepsilon_0 \varepsilon_r \frac{W}{h} \tag{3.19}$$

C_f is the fringe capacitance as if for an uncoupled single microstrip line, and is evaluated by [9],

$$2C_f = \sqrt{\varepsilon_{re}}/(cZ_c) - C_p \tag{3.20}$$

The term C'_f accounts for the modification of fringe capacitance C_f of a single line due to the presence of another line. An empirical expression for C'_f is given by [9],

$$C'_f = \frac{C_f}{1 + A(\frac{h}{s})\tanh\left(\frac{8s}{h}\right)} \tag{3.21}$$

$$\text{where, } A = \exp\left[-0.1\exp\left(2.33 - 2.53\frac{W}{h}\right)\right] \tag{3.22}$$

For the odd-mode, C_{ga} and C_{gd} represent, respectively, the fringe capacitances for the air and dielectric regions across the coupling gap. The capacitance C_{gd} may be found from the corresponding coupled strip line geometry, with the spacing between the ground planes given by $2h$. A closed-form expression for C_{gd} is,

$$C_{gd} = \frac{\varepsilon_0 \varepsilon_r}{\pi} \ln\left[\coth\left(\frac{\pi}{4}\frac{s}{h}\right)\right] + 0.65 C_f \left(\frac{0.02\sqrt{\varepsilon_r}}{s/h} + 1 - \frac{1}{\varepsilon_r^2}\right) \tag{3.23}$$

The capacitance C_{ga} can be modified from the capacitance of the corresponding coplanar strips, and expressed in terms of a ratio of two elliptic functions,

$$C_{ga} = \varepsilon_0 \frac{K(k')}{K(k)} \tag{3.24}$$

Where,

$$k = \frac{\frac{s}{h}}{\frac{s}{h} + 2\frac{W}{h}}$$

and, $k' = \sqrt{1-k^2}$

again,

$$\frac{K(k')}{K(k)} = \begin{cases} \dfrac{1}{\pi}\ln\left(2\dfrac{1+\sqrt{k'}}{1-\sqrt{k'}}\right) & \text{for } 0 \le k^2 \le 0.5 \\[2ex] \dfrac{\pi}{\ln\left(2\dfrac{1+\sqrt{k}}{1-\sqrt{k}}\right)} & \text{for } 0.5 \le k^2 \le 1 \end{cases} \tag{3.25}$$

After deriving C_o and C_e, we can derive Z_o and Z_e as follows,

$$Z_e = \frac{1}{c\sqrt{C_e^a C_e}} \tag{3.26}$$

$$Z_o = \frac{1}{c\sqrt{C_o^a C_o}} \tag{3.27}$$

Where, C_e^a and C_o^a are even and odd capacitance for the coupled microstrip line configuration with air as dielectric.

Now computing (3.15) and (3.16), we have,

$$\begin{bmatrix} \dfrac{Z_e+Z_o}{Z_e-Z_o} & -j\dfrac{2Z_eZ_o\cot\theta_e}{Z_e-Z_o} \\ j\dfrac{2}{Z_e\cot\theta_e-Z_o\cot\theta_o} & \dfrac{Z_e+Z_o}{Z_e-Z_o} \end{bmatrix} = \begin{bmatrix} 1+Z_gY_p & Z_g \\ Y_p(2+Z_gY_p) & 1+Z_gY_p \end{bmatrix} \tag{3.28}$$

Now, $-j\dfrac{2Z_eZ_o\cot\theta_e}{Z_e-Z_o} = \dfrac{1}{j\omega C_g}$

So,
$$C_g = \frac{Z_e-Z_o}{2\omega Z_eZ_o\cot\theta_e} \tag{3.29}$$

Then,

$$1+Z_gY_p = \frac{Z_e+Z_o}{Z_e-Z_o}$$

$$\Rightarrow 1+\left(-j\frac{2Z_eZ_o\cot\theta_e}{Z_e-Z_o}\right)j\omega C_p = \frac{Z_e+Z_o}{Z_e-Z_o}$$

$$\Rightarrow \frac{2Z_eZ_o\cot\theta_e}{Z_e-Z_o}\omega C_p = \frac{2Z_o}{Z_e-Z_o}$$

So,
$$C_p = \frac{1}{\omega Z_e\cot\theta_e} \tag{3.30}$$

Now, combining the equivalent circuits from Figure 3.6 and Figure 3.8, we get the equivalent circuit shown in Figure 3.10.

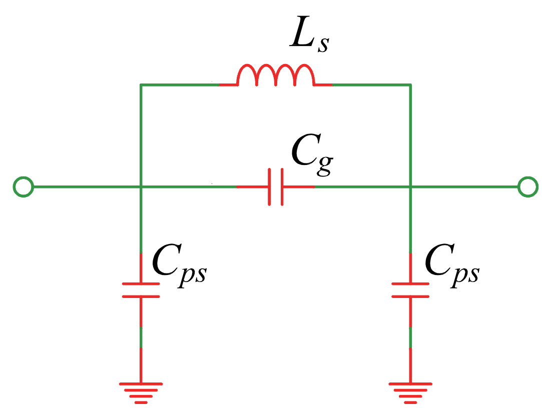

Figure 3.11 Equivalent circuit for SIR proposed by K. Cheng

This model has been proposed by K. Cheng [1] for the first time and was verified by MoM simulator and experimental data.

Here, the combined capacitance is given by,

$$C_{ps} = C_p + C_s + C_\Delta \tag{3.31}$$

Where, C_p=Capacitance of the single transmission line

C_s=Capacitance of the coupled line

C_Δ=Capacitance due to junction discontinuity

We have neglected the effect of the junction discontinuity because the value of C_Δ is negligible compared to C_p *and* C_s.

3.4 Modified Parallel Triangular Line

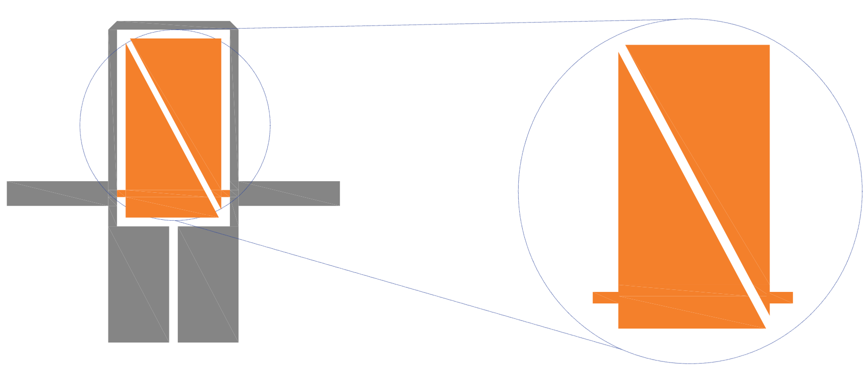

Figure 3.12 Modified triangular couple line

Figure 3.13 Modified triangular couple line simplification

The triangular plates inside the series line has capacitance other than the above mentioned abrupt stepped junction capacitance. For simplicity we can assume these two triangular plates as parallel coupled lines. For deriving purpose of the equivalent circuit we can assume the triangular couple line as parallel coupled lines shown in Figure 3.13. From the theory of microstrip line gap [21] we have the equivalent circuit shown in Figure 3.14.

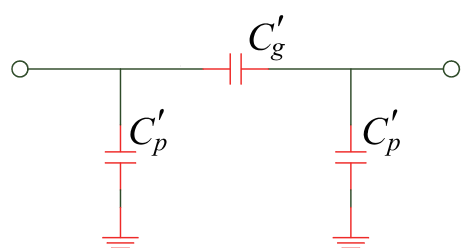

Figure 3.14 Equivalent circuit for the modified triangular couple line

Where,

$$C'_p = \frac{C_{even}}{2} \tag{3.32}$$

and

$$C'_g = \frac{C_{odd}}{2} - \frac{C_{even}}{4} \tag{3.33}$$

These capacitance will shift the spurious effect further more right, giving us a broad stopband. It also make the filter more compact than predicted by K. Chang et.al.[1]

3.5 Overall Equivalent Circuit

Now the overall equivalent circuit for the proposed modified stepped impedance resonator is shown in Figure 3.15.

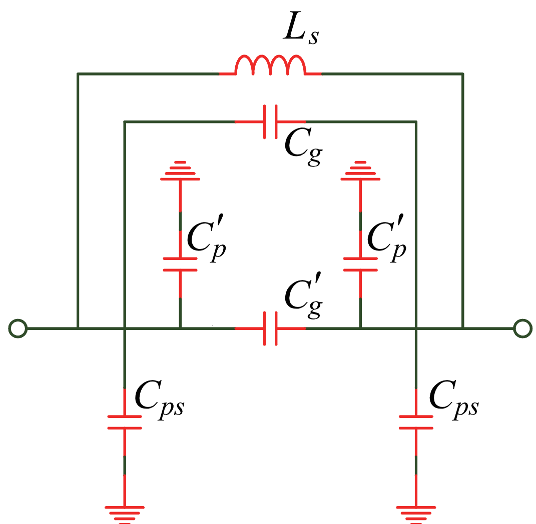

Figure 3.15 Equivalent circuit for the proposed filter in this thesis

3.6 Conclusion

In this chapter, the equivalent circuit for the proposed structure is derived. The total circuit is consisting of three major parts. The equivalent circuit of each individual part is derived separately and finally combined into one circuit. Here some of the components of the circuit is neglected for simplification. So the output of the filter will not be 100 percent correct, but it will be close to original response.

CHAPTER 4

NUMERICAL ANALYSIS

4.1 Introduction

Hairpin filters have greater inductance than parallel coupled filters. But it requires smaller space than normal parallel coupled half wavelength resonator filter or end couple half wavelength resonator filters. It has ‘U’ shaped inductor with parallel couple stepped inductance resonator. In this chapter we will show some filter structure and their EM simulation result using Advanced Design System (ADS) 2011.01 by Agilent system[23]. For every simulation the meshing is set for 20GHz to get the best result.

4.2 Stepped Impedance Hairpin Resonator

4.2.1 Single stepped impedance hairpin resonator

Figure 4.1 shows the structure of the stepped impedance hairpin resonator. As the line has a stepped impedance resonator, it has less space than conventional hairpin line resonator. K. Cheng [1] was first to include this stepped impedance to a conventional hairpin line resonator. The only purpose of the inclusion of the stepped impedance was to make the structure compact. There are 2 ports−port 1 and port 2 with feed line, l_f. The width of the feed line is w_1. Now we have matched the line with 50Ω input and output line. First, the series line has a length of l_s (l_2 +2 l_3 +2 w_1) and width of w_2.

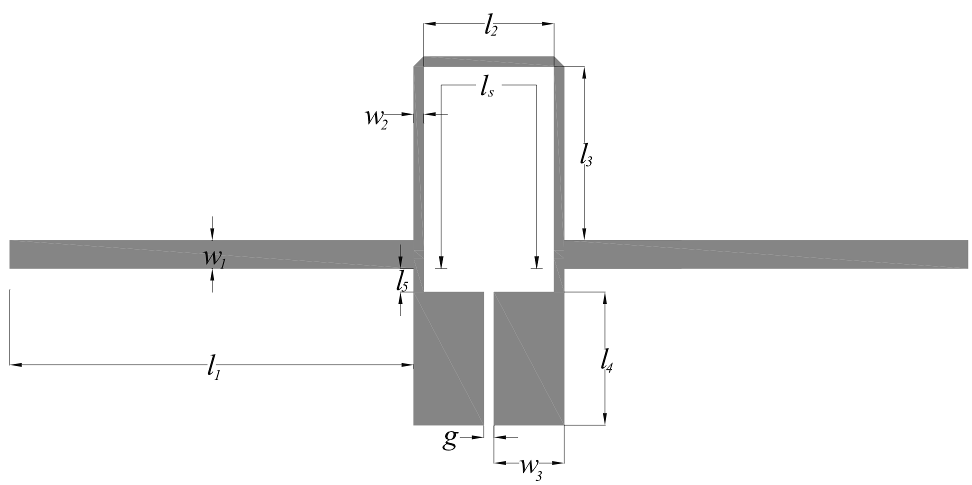

Figure 4.1 Layout of stepped-impedance hairpin resonator

As the length, $l_s = l_2 + 2l_3$ is larger than the width, w_2 , it shows good inductance. Then the parallel couple line has large width, w_3, length, l_4 and gap between parallel plates, g.

This lowpass filter is designed for a 3dB cut-off frequency of 1.86 GHz and fabricated on a 0.254mm thick RT/Duroid 5880 substrate with a dielectric constant ε_r=2.2. The dimensions considered in this modeling are as below:

l_1= 18mm and w_1=0.79mm for a 50Ω feed line to match the input and output port. l_2= 5mm, l_3= 5.3mm, l_4=6.2mm, l_5= 1mm,w_2=0.2mm, w_3=2.6mm and gap size g=0.2mm.

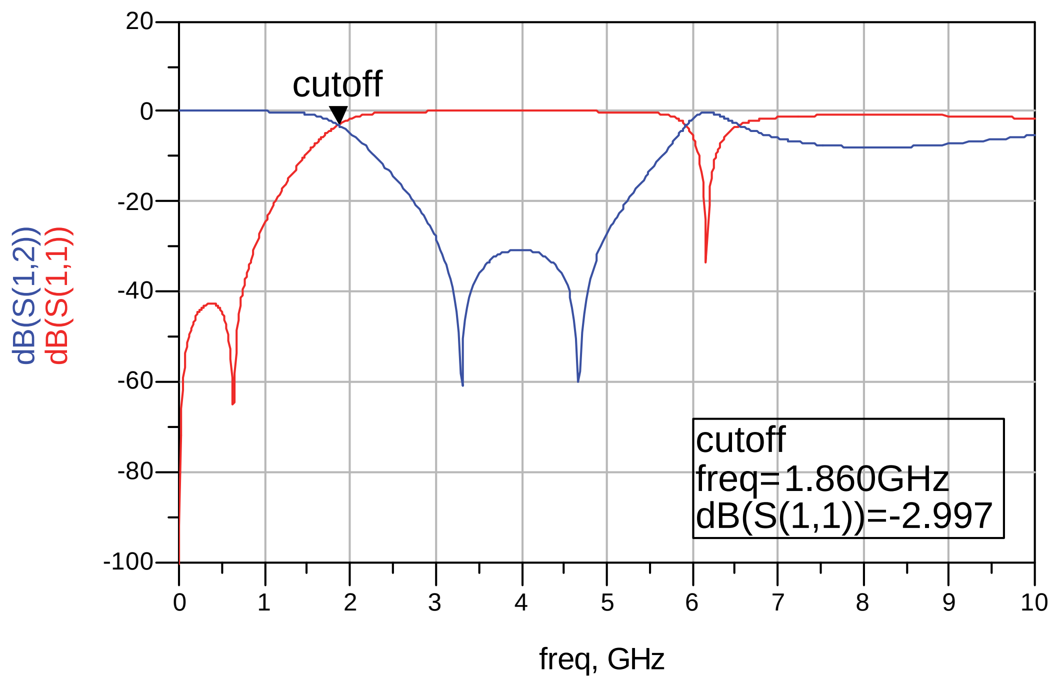

Figure 4.2 EM simulated results for the filter in Figure 4.1 where 1.86 GHz is the cutoff frequency

Figure 4.2 shows the S_{11} and S_{12} parameter. It has a cut-off 1.86GHz, a transmission Zero at 700MHz before cut-off and two spurious zero(3.3GHz and 4.7GHz) after cut-off inside the stopband. Here the stop band is 1.7GHz to 5.95GHz. It also shows that there is a spurious pole at 6.2GHz. Here insertion loss is −43dB which is good.The rejection rate is 22dB/GHz, and at stopband, the rejection is of -30dB.

4.2.2 Cascaded stepped impedance hairpin resonator varying width

Figure 4.3 figure shows five multiple cascaded stepped impedance hairpin resonators. Two resonators are linked with an adjacent transmission line $w_{7,}$ $w_{8,}$ w_9 and w_{10}. Due to the adjacent transmission line, the coupled lines become an asymmetrical coupling structure, as shown on the left-hand side of Figure 4.3(b). The asymmetrical coupled lines can roughly be treated as a symmetric coupled line with a separate parallel single transmission line as shown on the right-hand side of Figure 4.3(b) [16]. Here the dimensions are, l_1=18mm l_4=6.2mm, w_1=0.79mm w_2=0.2mm, w_3=2.6mm, w_7=0.7mm, w_8=1.4mm, w_9=2.1mm, w_{10}=2.8mm and g=0.2mm.

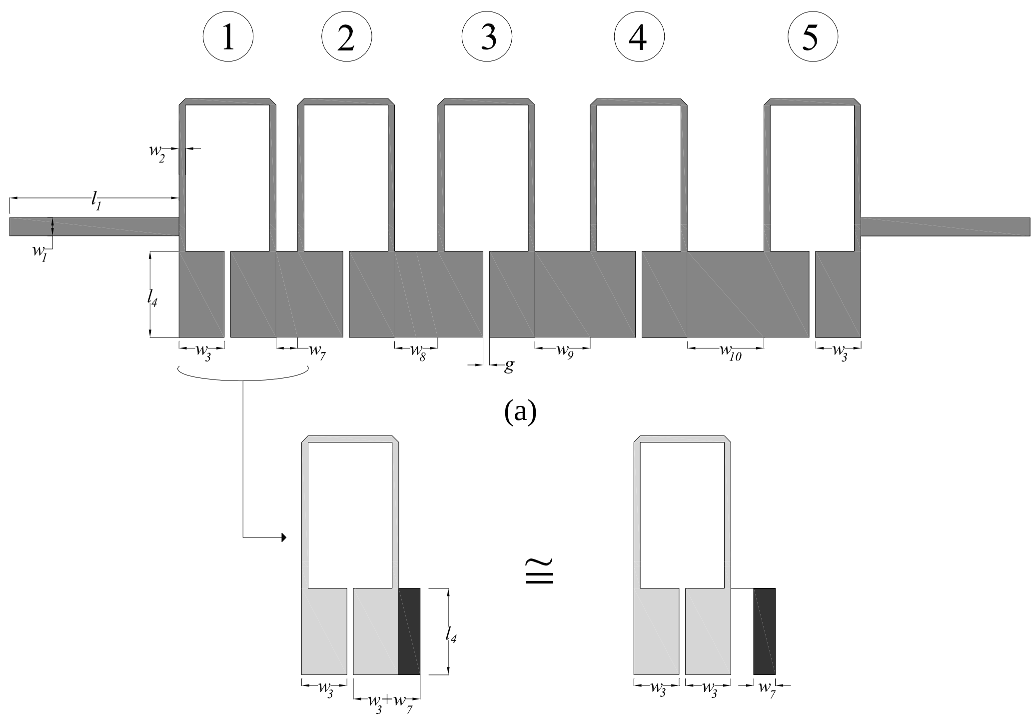

(b)

Figure 4.3 Layout of cascaded stepped impedance resonator with variation of width

As changing width of the adjacent transmission line, the capacitance of the cascaded circuit will change its resonant frequencies. Resonant frequency depends on the size of the filter. So there are five resonant frequencies which are asymmetric parallel coupled line.

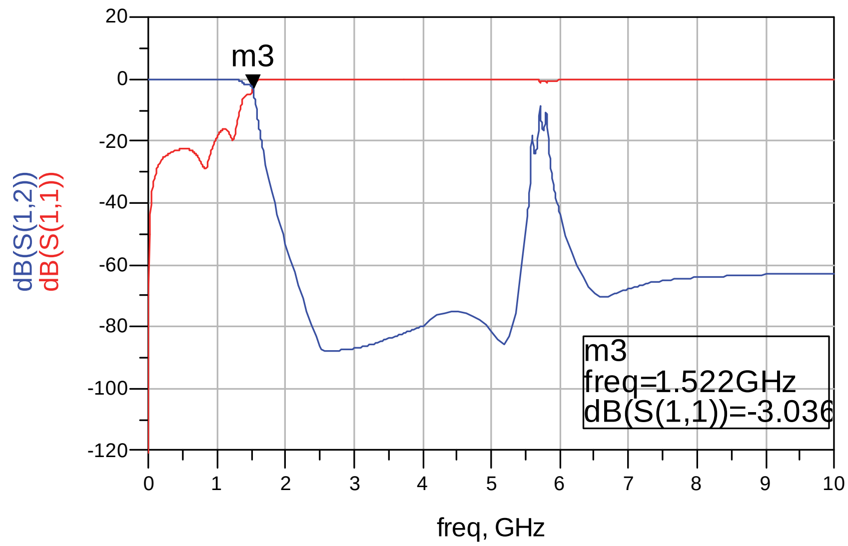

Figure 4.4 EM simulated results for the filter in Figure 4.3 where 1.522 GHz is the cutoff frequency

We have assumed it as symmetric parallel coupled line for simplicity. The cut-off frequency depends on the left most hairpin structure which has the highest cut-off frequency. So, the rejection region deviates to −80dB and rejection rate is 84dB/GHz just after the cut-off. It seems that the cascaded circuit has three times greater rejection than single one.

4.2.3 Cascaded stepped impedance hairpin resonator varying length

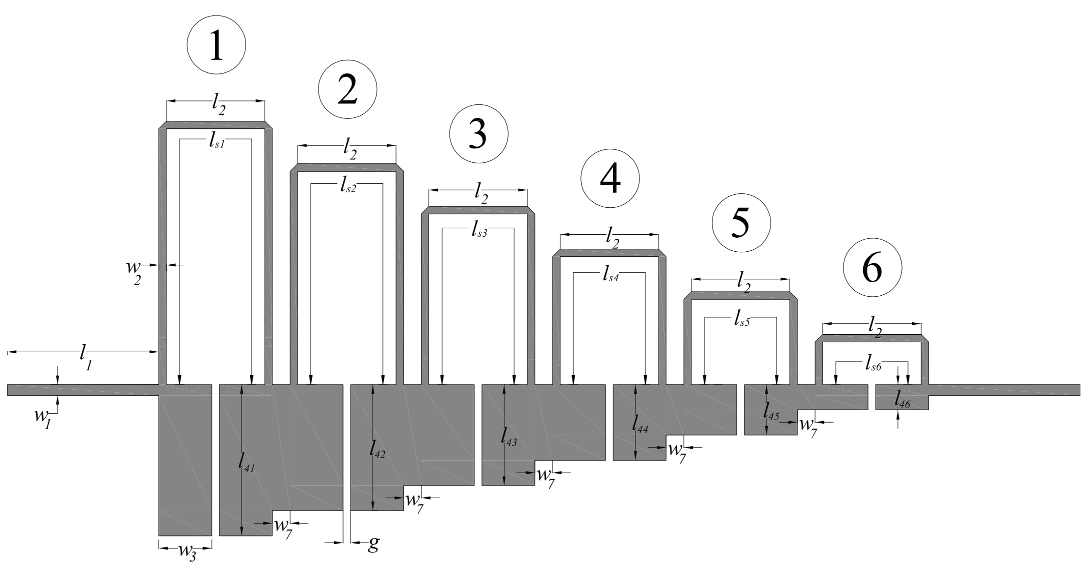

Figure 4.5 Layout of cascaded stepped impedance resonator with variation of length

Figure 4.5 shows six cascaded stepped impedance hairpin resonators varying the length of the resonators, keeping the width same. By varying the length the resonant frequency can be changed more than changing the width of the stepped impedance filters. For this particular case, l_1=18mm, l_2=5mm, l_{s1}=48mm, l_{s2}=32mm, l_{s3}=22.4mm, l_{s4}=16mm, l_{s5}=12.8mm, l_{s6}=8mm, l_{41}=18.6mm, l_{42}=11.2mm, l_{43}=8.7mm, l_{44}=6.2mm, l_{45}=5mm, l_{46}=3.1mm, and w_1=0.79mm, w_2=0.2mm, w_3=2.6mm,, w_7=0.7mm, and g=0.2mm.

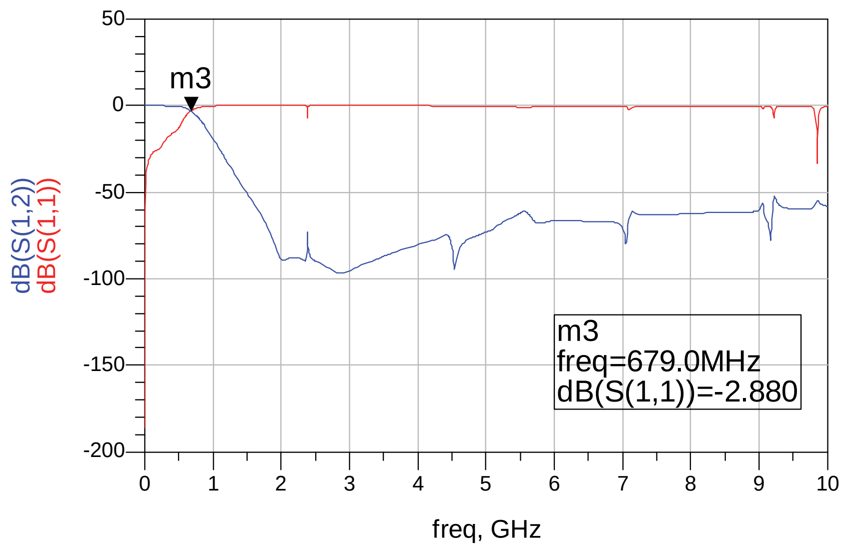

Figure 4.6 EM simulated results for the filter in Figure 4.5 where 679 MHz is the cutoff frequency

Here the stopband rejection is of -70dB after 1.7GHz and rejection rate is 66dB/GHz. The cut-off frequency is 679.5MHz which depends on the largest stepped impedence hairpin filter . As the length become smaller, the frequency shifts toward the right of the cut-off.

4.2.4 Single modified stepped impedance hairpin resonator proposed in [5]

Figure 4.7 shows the proposed stepped impedance hairpin resonator in [5]. An extra capacitor was included inside the hairpin structure. The low pass filter was designed for a 3dB cut-off frequency of 1.516 GHz and fabricated on a 0.254mm thick RT/Duroid 5880 substrate with a relative dielectric constant ε_r=2.2. The dimensions considered in this modeling are as below:

l_1=18mm and w_1=0.79mm for a 50Ω feed line to match the input and output port. l_2=5mm, l_3=5.3mm, l_4=6.2mm, l_5=1.0mm, l_6=6.5mm, w_2=0.2mm, w_3=2.6mm, w_4=0.2mm, w_5=0.4mm, w_6=0.2mm and gap size g=0.2mm.

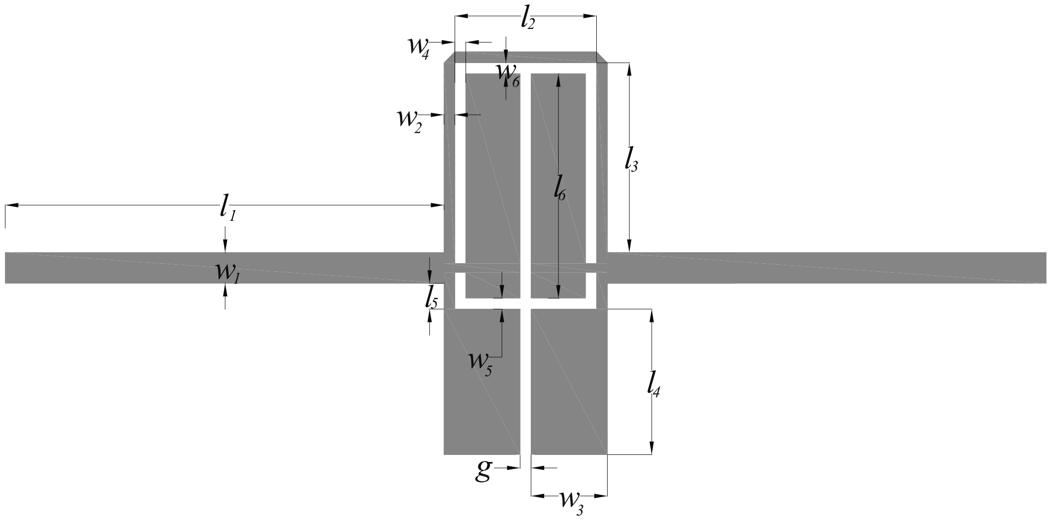

Figure 4.7 Layout of proposed modified stepped-impedance hairpin resonator in [5].

.

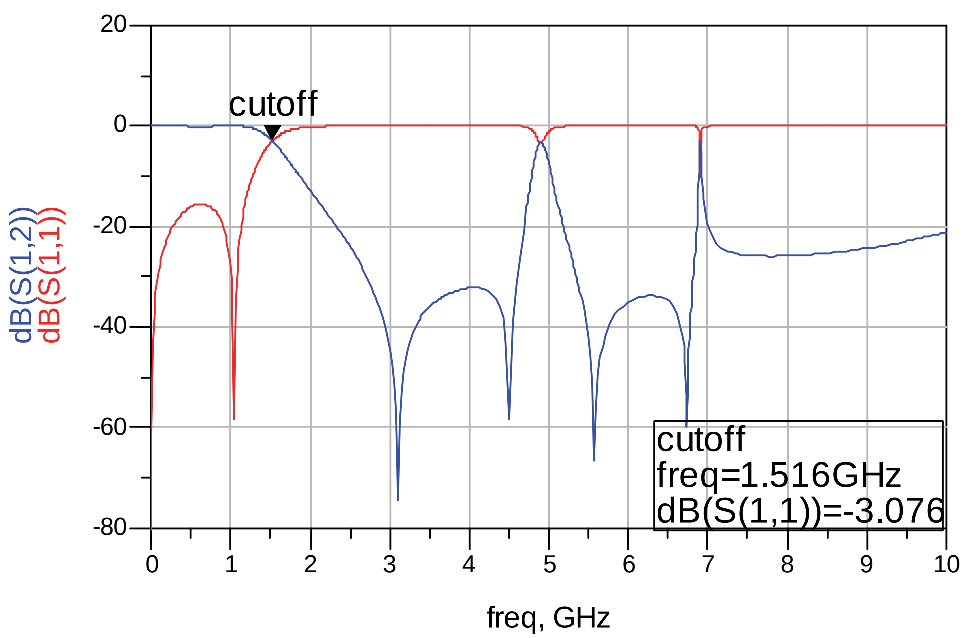

Figure 4.8 EM simulated results for the filter in Figure 4.7 where 1.516 GHz is the cutoff frequency

Figure 4.8 shows the S_{11} and S_{12} parameter for the filter shown in Figure 4.7. It has cut-off frequency at 1.516 GHz, a transmission zero at 1.05GHz before cut-off and four spurious zeros (3.1GHz, 4.5GHz, 5.6GHz and 6.8GHz) after cut-off inside the stopband. There are two major spurious effects at 4.9GHz and 6.95GHz. Here insertion loss is −18dB. The rejection rate is 29dB/GHz, and at stopband the rejection is of −30dB.

4.3 Proposed Modified Stepped Impedance Hairpin Resonator

4.3.1 Single proposed modified stepped impedance hairpin resonator

Figure 4.9 shows the proposed structure in this thesis. Here two extra triangular capacitors are included inside the hairpin structure. The coupled stepped impedance resonators are used as a capacitor in order to get a sharp cutoff frequency response and create a pole at harmonic to get a broad stopband. As this extra parallel coupled resonator will create an extra pole at harmonic, it will suppress the higher order spurious mode. Thus the modification of the stopband can be made. The filter will be compact because the extra capacitor is introduced inside of the filter which was unutilized.

The low pass filter has been designed for a 3dB cut-off frequency of 1.518 GHz and fabricated on a 0.254mm thick RT/Duroid 5880 substrate with a relative dielectric constant ε_r=2.2. The dimensions considered in this modeling are as follows: l_1= 18mm and w_1=0.79mm for a 50Ω feed line to match the input and output port, l_2= 5mm, l_3=5.3mm, l_4=6.2mm, l_5=1mm, l_6=6.5mm, w_2=0.2mm, w_3=2.6mm, w_4=0.2mm, w_5=0.4mm, w_6=0.2mm and gap size g=x=0.2mm.

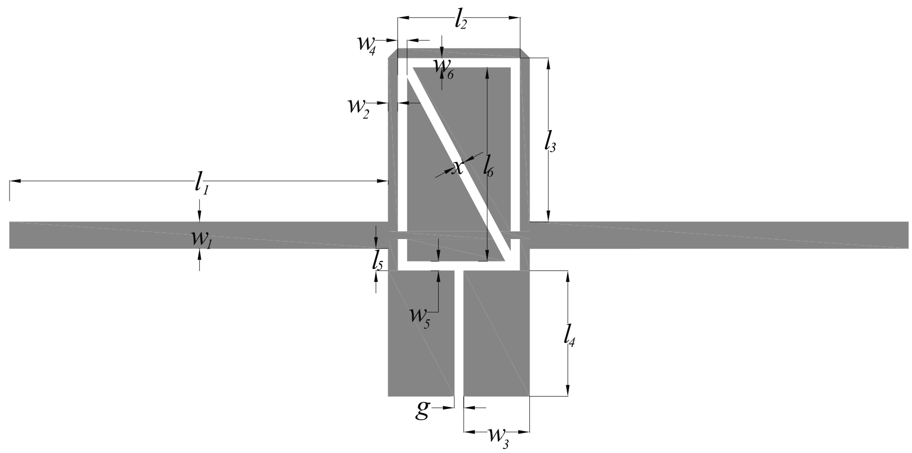

Figure 4.9 Layout of proposed modified stepped-impedance hairpin resonator.

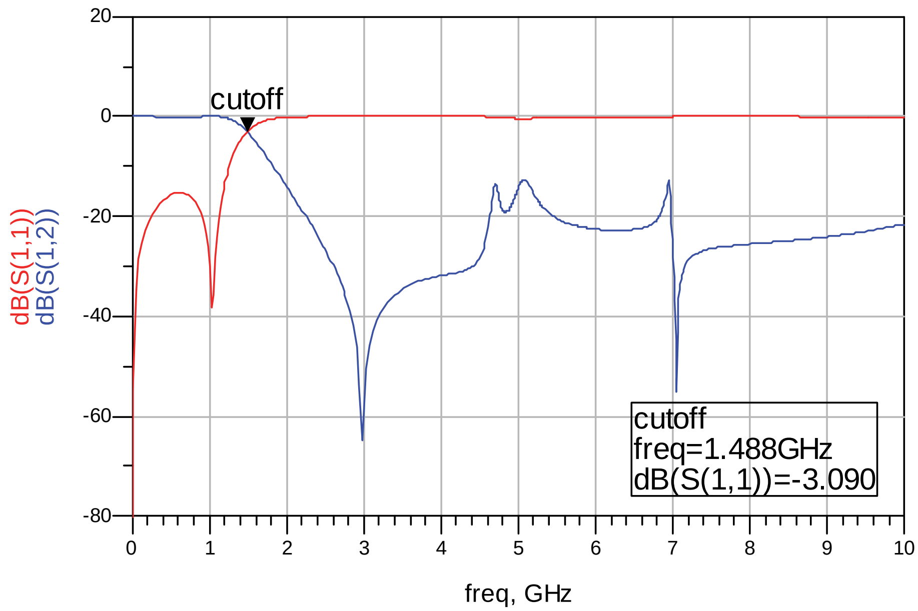

.

Figure 4.10 EM simulated results for the filter in Figure 4.9 where 1.488 GHz is the cutoff frequency

Figure 4.10 shows the S_{11} and S_{12} parameter for the filter shown in Figure 4.9. It has a cut-off frequency at 1.488 GHz, a transmission Zero at 1.05GHz before cut-off and three spurious zeros (3.0GHz, 5.8GHz and 6.95GHz) after cut-off inside the stopband. The filter shows a very good stopband from 1.488GHz to 12.5GHz. Here insertion loss is −18dB. The rejection rate is 27.8dB/GHz, and at stopband the rejection is of -28dB.

4.3.2 Cascaded proposed modified SIR hairpin filter varying width

Figure 4.11 shows five multiple cascaded modified stepped impedance hairpin resonators. Two resonators are linked with by an adjacent transmission line with w_7, w_8, w_9 and w_{10}. Due to the adjacent transmission line, the coupled lines become an asymmetrical coupling structure, as shown on the left-hand side of Figure 4.11(b). The asymmetrical coupled lines can be roughly treated as a symmetric coupled line with a separate parallel single transmission line, as shown on the right-hand side of Figure 4.11(b) [16].Here the dimensions are, l_1=18mm l_4=6.2mm, w_1=0.79mm w_2=0.2mm, w_3=2.6mm, w_4=0.2mm, w_5=0.4mm, w_6=0.2mm, w_7=0.7mm, w_8=1.4mm, w_9=2.1mm, w_{10}=2.8mm and g=x=0.2mm.

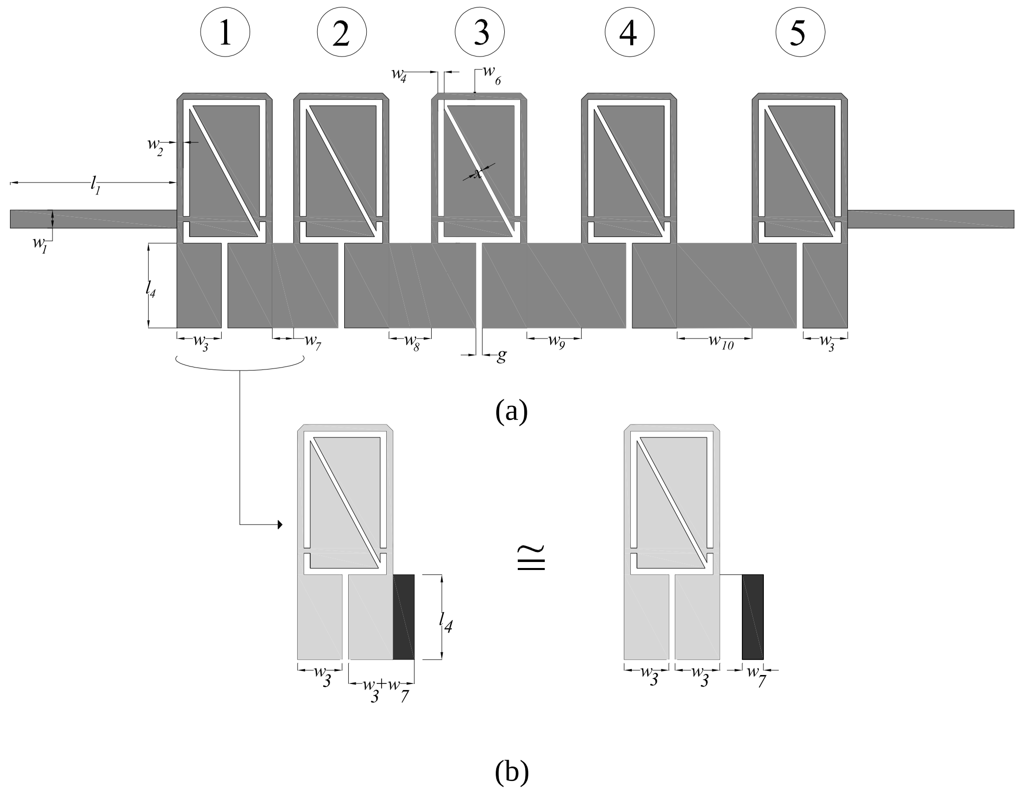

Figure 4.11 Layout of cascaded modified stepped impedance resonator with variation of width

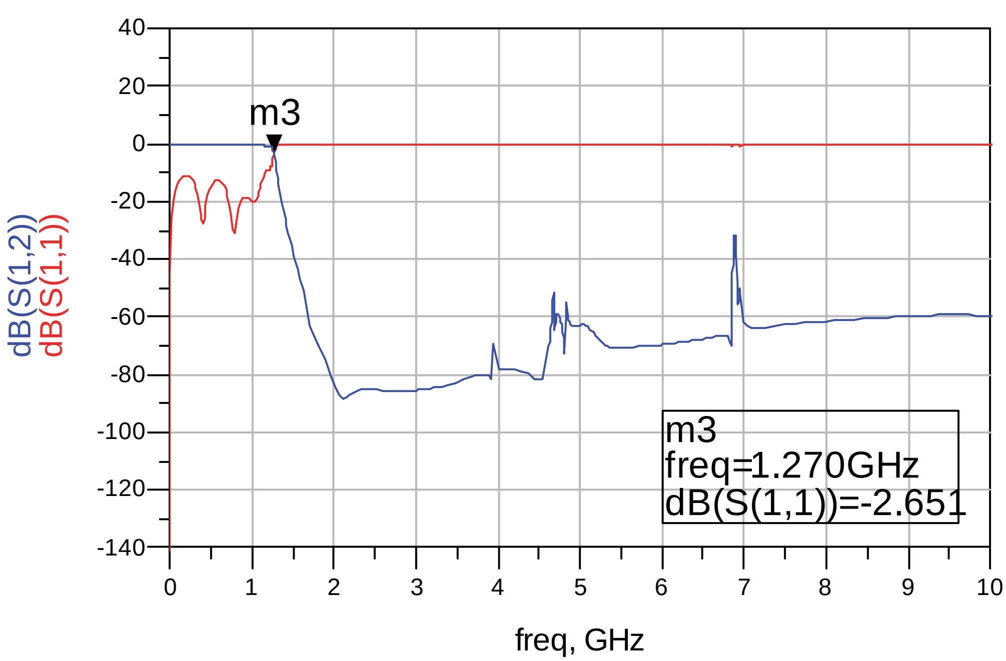

Figure 4.12 EM simulated results for the filter in Figure 4.11 where 1.270 GHz is the cutoff frequency

As changing width of the adjacent transmission line, the capacitance of the cascaded circuit will change its resonant frequencies. Resonant frequency depends on the size of the filter. So there are five resonant frequencies which are asymmetric parallel coupled line. We have assumed it as symmetric parallel coupled line for simplicity. The cut-off frequency depends on the left most hairpin structure. So, the rejection region deviates to -85dB and rejection rate is 96.2dB/GHz just after the cut-off, which is very steep. It seems that the cascaded circuit has four times greater rejection than single one. So any rejection and rejection rate can be designed with cascading the proper number of stepped impedance hairpin resonator.

4.3.3 Cascaded proposed modified SIR hairpin filter varying length

Figure 4.13 shows six cascaded modified stepped impedance hairpin resonators varying the length of the resonators, keeping the width same. By varying the length, we can modify the resonant frequency more than changing the width of the stepped impedance filters. For this particular case we took, l_1=18mm, l_2=5mm, l_{s1}=48mm, l_{s2}=32mm, l_{s3}=22.4mm, l_{s4}=16mm, l_{s5}=12.8mm, l_{s6}=8mm, l_{41}=18.6mm, l_{42}=11.2mm, l_{43}=8.7mm, l_{44}=6.2mm, l_{45}=5mm, l_{46}=3.1mm, and w_1=0.79mm, w_2=0.2mm, w_3=2.6mm,, w_7=0.7mm, and g= x=0.2mm.

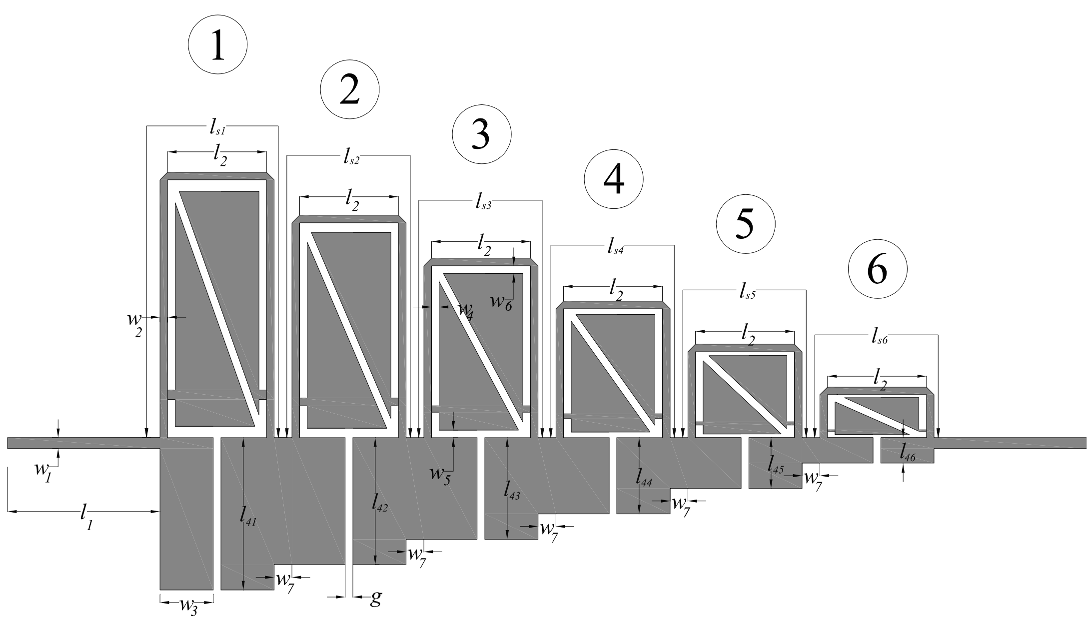

Figure 4.13 Layout of cascaded modified stepped impedance resonator with variation of length

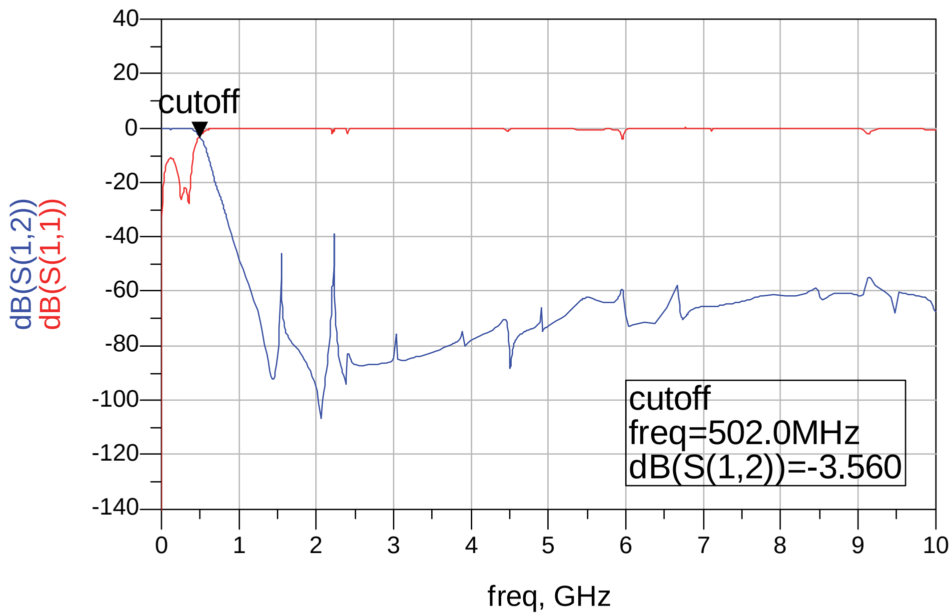

Figure 4.14 EM simulated results for the filter in Figure 4.13 where 502MHz is the cutoff frequency

Here we have rejection of -82dB and rejection rate is 105dB/GHz just after cut-off. Its cut off frequency is 502MHz which depends on the left most (largest) modified stepped impedance hairpin filter. As the length become smaller, the frequency shifts toward the right of the cut-off.

4.3.4 Single modified stepped impedance hairpin resonator varying length

Now we take another case where we take the structure described in 4.3.1 and vary the l_3 and l_6. For this case we take l_3= 6.1mm and l_6= 7.3mm

So the dimensions become, l_1= 18mm and w_1=0.79mm for a 50Ω feed line to match the input and output port. l_2= 5mm, l_3= 6.1mm, l_4=6.2mm, l_5= 1mm, l_6= 7.3mm, w_2=0.2mm, w_3=2.6mm, w_4=0.2mm, w_5=0.4mm, w_6=0.2mm and gap size $g = x = 0.2$mm.

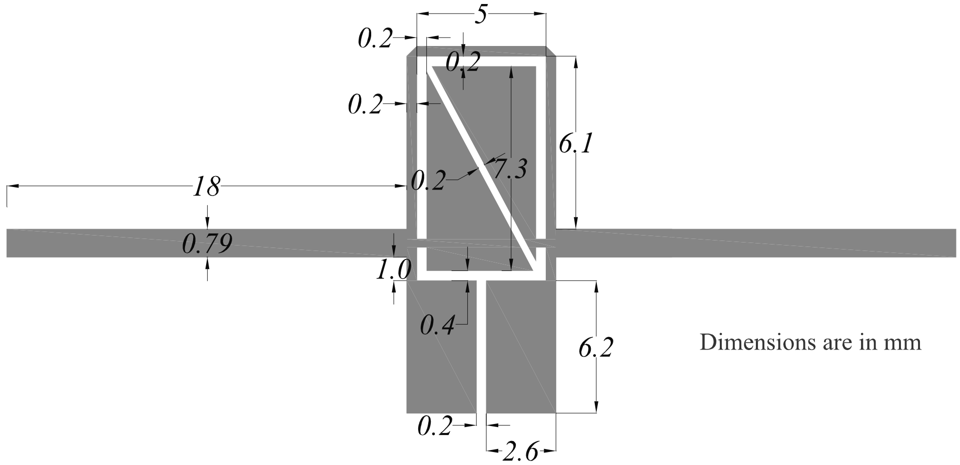

Figure 4.15 Layout of modified stepped-impedance hairpin resonator in 4.3.4.

Figure 4.16 shows the S_{11} and S_{12} parameter for the filter shown in Figure 4.15. Increasing the length (l_3 and l_6) of the modified SIR filter decreases the cutoff frequency. As the size of the filter increases, the cut-off frequency of the filter decreases. The spurious effects also shift toward left. But the rejection and the rejection rate stays the same. The cut-off frequency is at 1.389GHz. The rejection rate becomes 31dB/GHz and the rejection at stopband is -30.7dB.

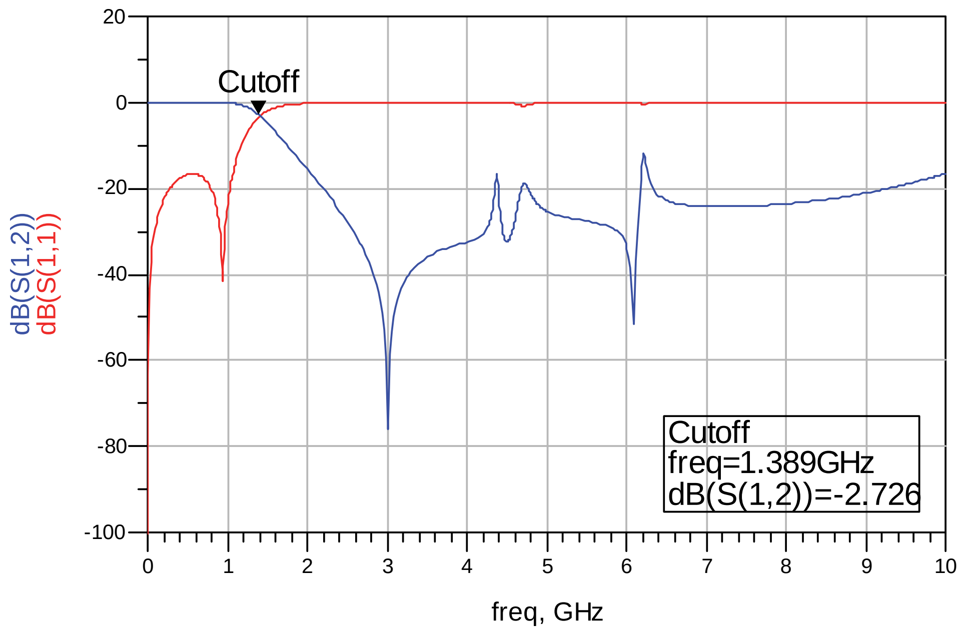

Figure 4.16 EM simulated results for the filter in Figure 4.15 where 1.389 GHz is the cutoff frequency

4.3.5 Single modified stepped impedance hairpin resonator varying width

Now we take another case where we take the structure described in 4.3.1 and vary the l_3 and l_6. For this case we take l_2= 4.2mm and w_3= 2.2mm. So the dimensions become, l_1= 18mm and w_1=0.79mm for a 50Ω feed line to match the input and output port. l_2= 4.2mm, l_3= 5.3mm, l_4=6.2mm, l_5= 1mm, l_6= 6.5mm, w_2=0.2mm, w_3=2.2mm, w_4=0.2mm, w_5=0.4mm, w_6=0.2mm and gap size g= x =0.2mm.

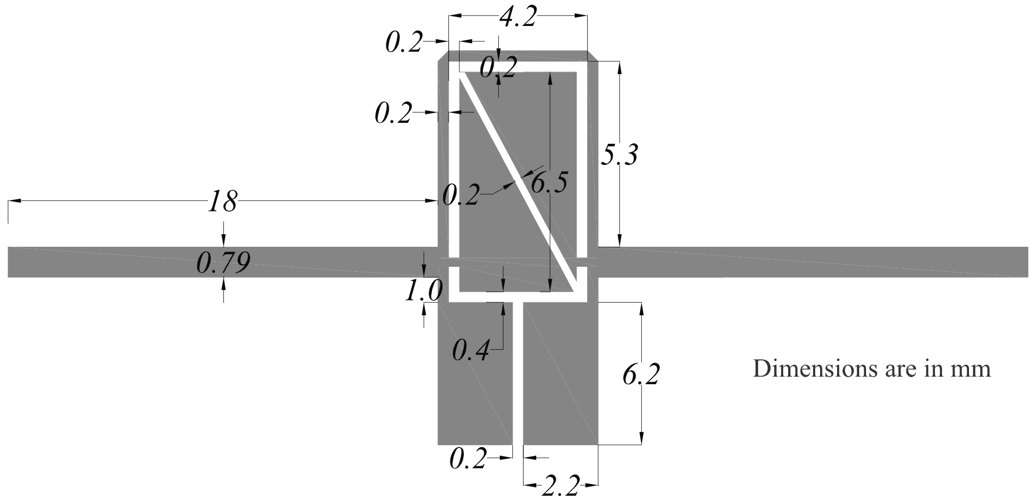

Figure 4.17 Layout of modified stepped-impedance hairpin resonator in 4.3.5.

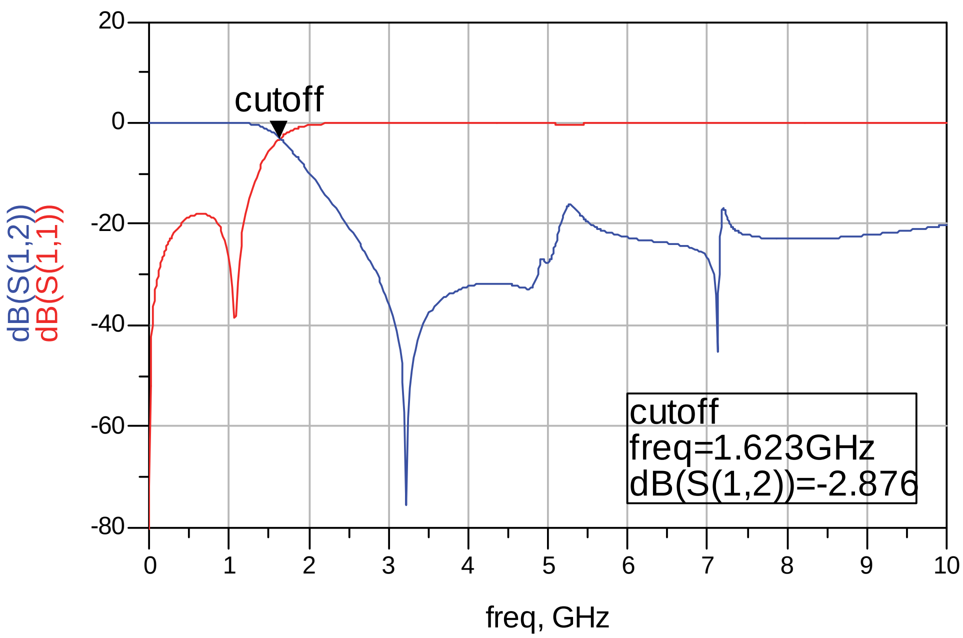

Figure 4.18 EM simulated results for the filter in Figure 4.17 where 1.623 GHz is the cutoff frequency.

Figure 4.18 shows the S_{11} and S_{12} parameter for the filter shown in Figure 4.17. Decreasing the width (l_2 and w_3) of the modified SIR filter decreases the cutoff frequency. As the size of the filter increases, the cut-off frequency (1.623GHz) of the filter decreases. The spurious effects also shift toward left. But the rejection and the rejection rate stays the same.

4.3.6 Single modified stepped impedance hairpin resonator varying gap

Now we take another case where we take the structure described in 4.3.1 and vary the g and x. For this case we take g= x= 0.4mm

l_1= 18mm and w_1=0.79mm for a 50Ω feed line to match the input and output port. l_2= 5.2mm, l_3= 5.3mm, l_4=6.2mm, l_5= 1mm, l_6= 6.5mm, w_2=0.2mm, w_3=2.6mm, w_4=0.2mm, w_5=0.4mm, w_6=0.2mm and gap size g= x= 0.4mm.

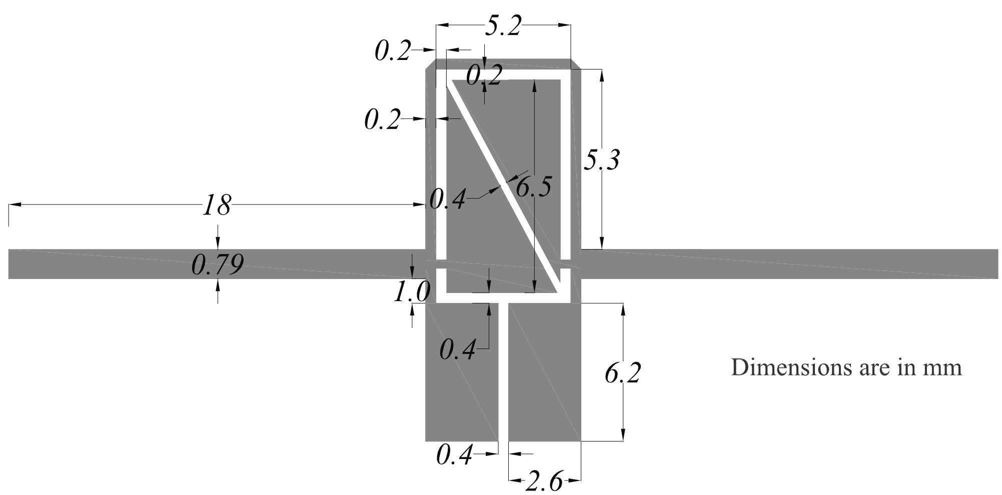

Figure 4.19 Layout of modified stepped-impedance hairpin resonator in 4.3.6

Figure 4.20 shows the S_{11} and S_{12} parameter for the filter shown in Figure 4.19. Increasing the gap g of the modified SIR filter increases the cutoff frequency slightly at 1.518GHz. The rejection attenuation decreases and rejection rate becomes25dB/GHz. But the spurious effect at 6.95GHz is increased.

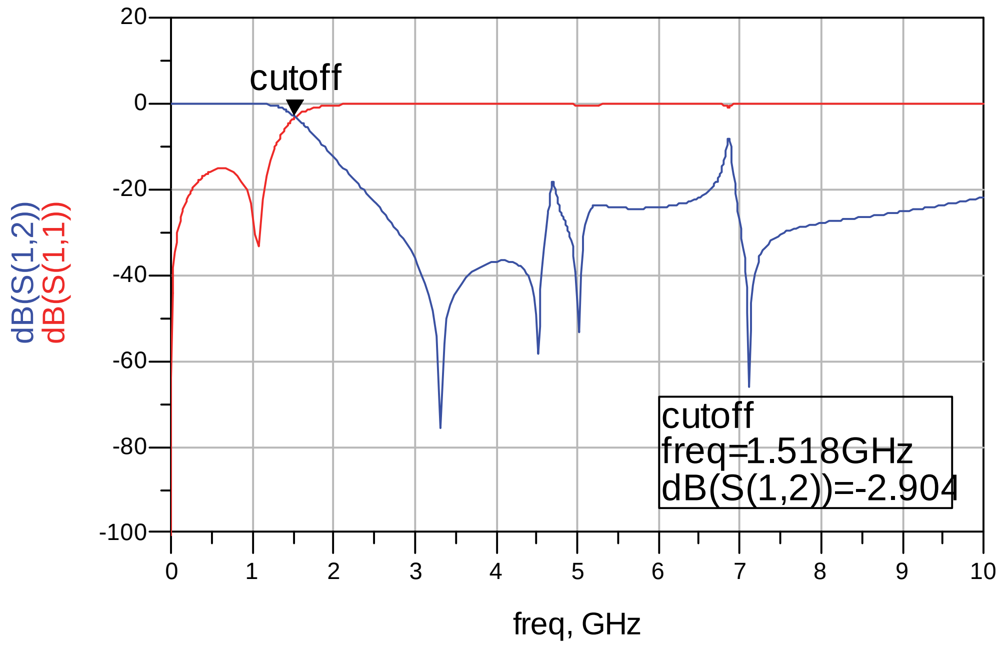

Figure 4.20 EM simulated results for the filter in Figure 4.19 where 1.518GHz is the cutoff frequency

4.3.7 Single modified stepped impedance hairpin resonator adjusting for high frequency

Now we take another case where we take the structure described in 4.3.1 and vary all the parameter to make the filter to have a cutoff frequency of 5 GHz.

l_1= 18mm and w_1=0.79mm for a 50Ω feed line to match the input and output port. l_2= 2.2mm, l_3= 1.4mm, l_4=2mm, l_5= 1mm, l_6= 2.6mm, w_2=0.2mm, w_3=1.2mm, w_4=0.2mm, w_5=0.4mm, w_6=0.2mm and gap size g=0.2mm, x= 0.2mm.

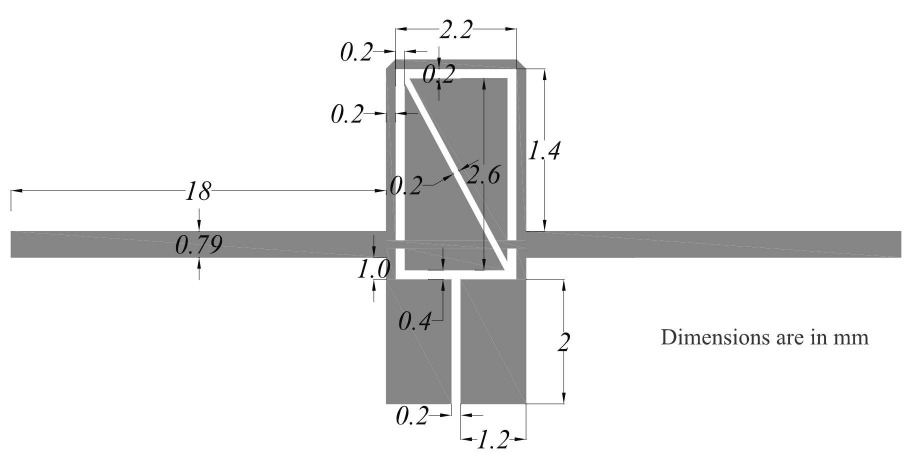

Figure 4.21 Layout of modified stepped-impedance hairpin resonator for 4.3.7

Figure 4.22 shows the S_{11} and S_{12} parameter for the filter shown in Figure 4.21. Here the 3dB cut-off frequency is 5 GHz. The rejection rate is 9dB/GHz. We have the stopband rejection at -24dB. Comparing to the lower frequency filters, the rejection rate of this filter is low. It has a rejection better than 10.2 dB from 6.2GHz to 22GHz. So the stopband is very broad.

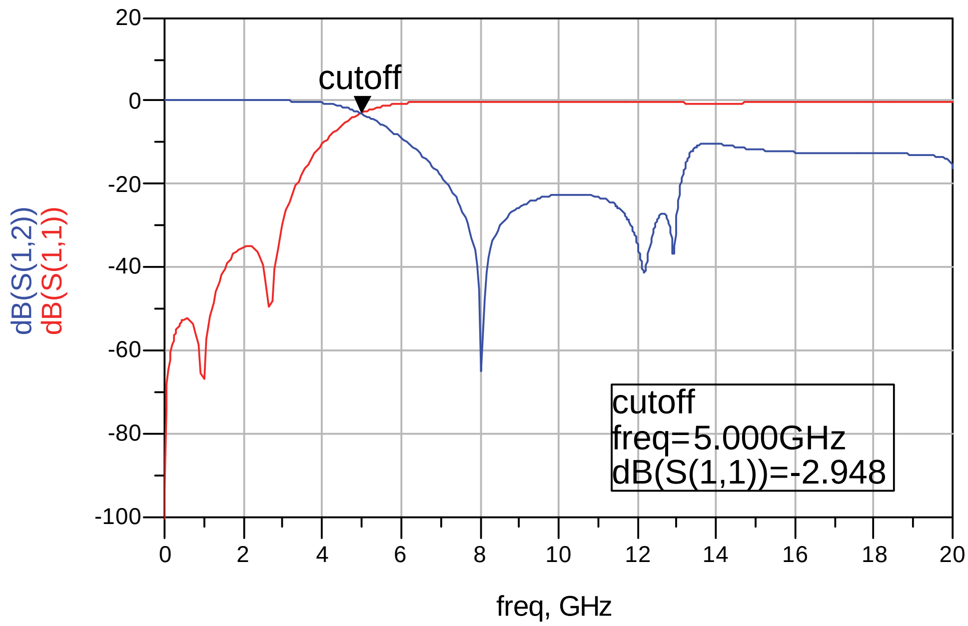

Figure 4.22 EM simulated results for the filter in Figure 4.21 where 5GHz is the cutoff frequency

Table 4.1 Relation between filter parameters and cut-off frequency

Parameters			Cut-off Frequency
l_s	series line length	Increase (↑)	Decrease (↓)
		Decrease (↓)	Increase (↑)
w_s	series line width	Increase (↑)	Increase (↑)
		Decrease (↓)	Decrease (↓)
l_c	Parallel couple line length	Increase (↑)	Decrease (↓)
		Decrease (↓)	Increase (↑)
w_c	Parallel couple line width	Increase (↑)	Decrease (↓)
		Decrease (↓)	Increase (↑)
g, x	Coupling gap	Increase (↑)	Increase (↑)
		Decrease (↓)	Decrease (↓)
h	Thickness of the substrate	Increase (↑)	Increase (↑)
		Decrease (↓)	Decrease (↓)
ε_r	dielectric constant	Increase (↑)	Decrease (↓)
		Decrease (↓)	Increase (↑)

4.4 Conclusion

In this chapter the layout simulation of the proposed filter and its variants are showed. From the simulations, many concluding decision can be taken. The cut-off frequency of the filter is inversely related with the series line length $l_{s.}$ But cut-off frequency increases with the increase of series line width $w_{s.}$ For the parallel coupled line both the width w_c and length l_c are inversely related with the cut-off frequency. But cut-off frequency increases with the increase with the coupling gap g. All of these relations are shown in Table 4.1. These relations can be uses to modify the cut-off frequency of the proposed filter and adjust it to any particular frequency. In this thesis the filter is modeled up to 5 GHz cut-off frequency lowpass response. As the cut-off frequency increases, the rejection rate after cut-off frequency decreases. For the proposed filter, the highest rejection rate can be obtained at the lower cut-off frequencies.

CHAPTER 5

CIRCUIT ANALYSIS

5.1 Introduction

The equivalent circuit of the proposed filter is shown in Figure 5.1.

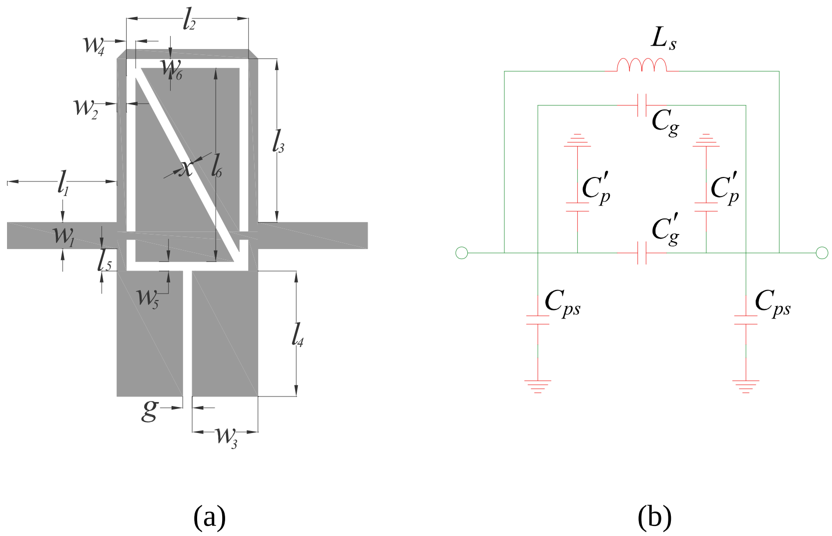

Figure 5.1 proposed SIR filter (a) structure, (b) equivalent circuit

The element of the equivalent circuits are directly depends on the dimension and the material of filter. These elements can be derived from the following equation derived previously,

$$L_s = \frac{Z_s \sin(\beta_s l_s)}{\omega} \quad (\mathrm{H}) \tag{5.1}$$

$$C_s = \frac{1-\cos(\beta_s l_s)}{\omega Z_s \sin(\beta_s l_s)} \quad (\mathrm{F}) \tag{5.2}$$

$$C_g = \frac{Z_o - Z_e}{2\omega Z_o Z_e \cot(\beta_c l_c)} \quad (\mathrm{F}) \tag{5.3}$$

$$C_p = \frac{1}{\omega Z_e \cot(\beta_c l_c)} \quad (\mathrm{F}) \tag{5.4}$$

$$C_{ps} = C_p + C_s \quad (\mathrm{F}) \tag{5.5}$$

$$C'_p = \frac{C_{even}}{2} \quad (\mathrm{F}) \tag{5.6}$$

$$C'_g = \frac{C_{odd}}{2} - \frac{C_{even}}{4} \quad (\mathrm{F}) \tag{5.7}$$

5.2 Equivalent Circuits for the Proposed Filters

5.2.1 Single proposed modified stepped impedance hairpin resonator

For the proposed modified stepped impedance resonator filter described in section 4.3.1 where, l_1=18mm, l_2=5mm, l_3=5.3mm, l_4=6.2mm, l_5=1mm, l_6=6.5mm, w_1=0.79mm, w_2=0.2mm, w_3=2.6mm, w_4=0.2mm, w_5=0.4mm, w_6=0.2mm x=0.2mm and gap size g=0.2mm, using the (5.1)-(5.7) the equivalent circuit is shown in Figure 5.2.

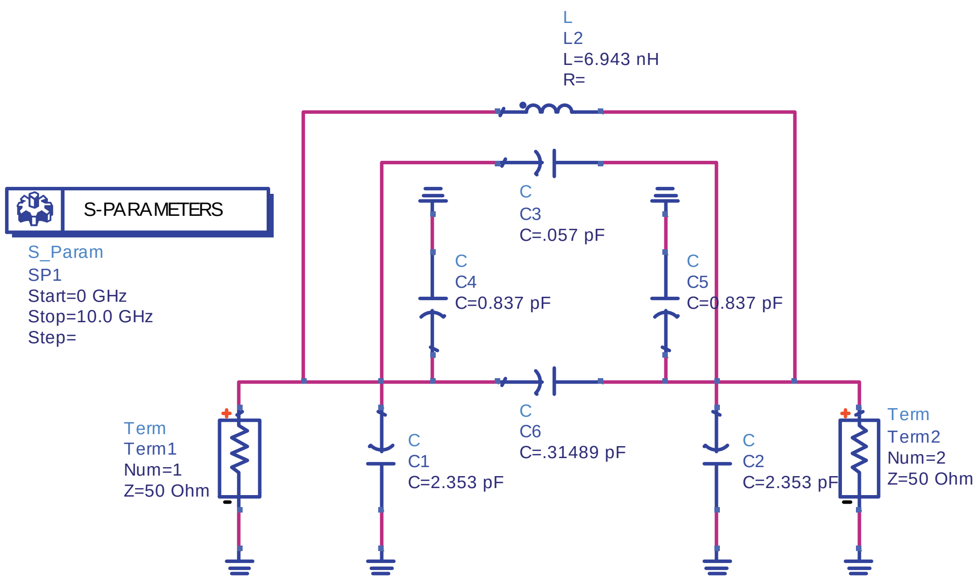

Figure 5.2 Equivalent circuit for the filter in Figure 4.9

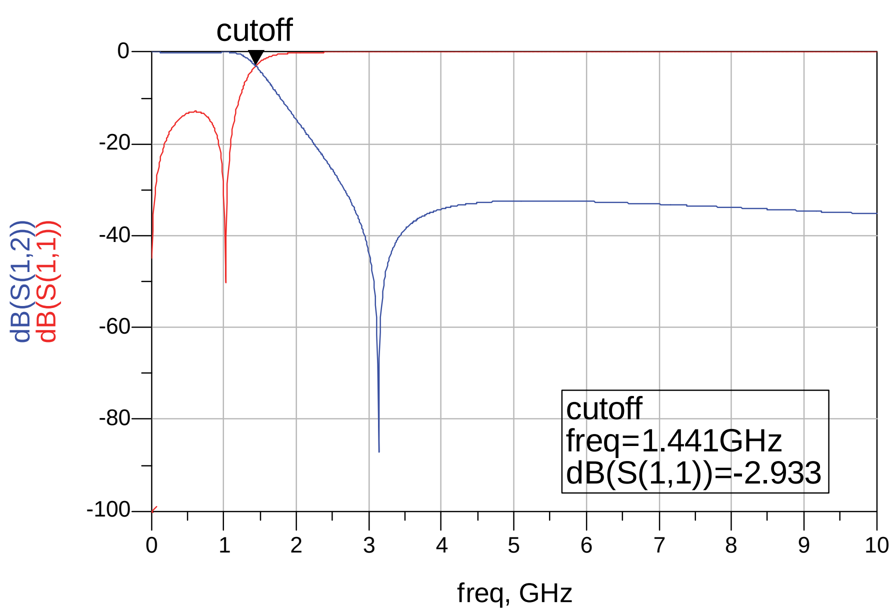

Figure 5.3 Output of the equivalent circuit of Figure 5.2

The S_{11} and S_{12} of the equivalent circuit is shown in the Figure 5.3. It has the cut-off frequency at 1.441GHz. As we used the first order Pi-model with modified capacitance (gap-capacitance), we cannot approximate the higher order resonant pole-zeroes with this simplified circuit. Here, form the figure we find that the rejection rate is 27dB/GHz, and at stopband the rejection is of -33dB.

So the equivalent circuit show good approximation with the layout simulation for cutoff frequency, rejection rate and stopband rejection.

5.2.2 Cascaded proposed modified SIR hairpin filter varying width

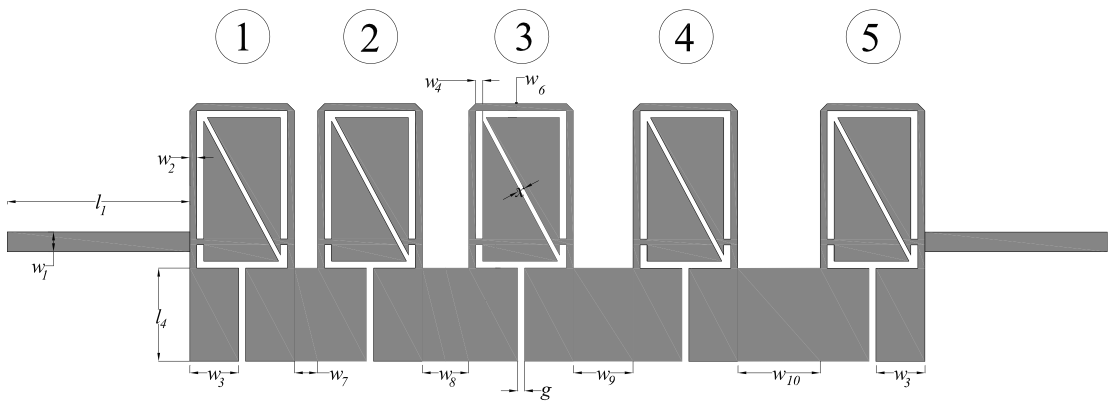

Figure 5.4 Layout of cascaded modified stepped impedance resonator with variation of width

For cascaded modified stepped impedance hairpin resonators with variable width, let two resonators are linked with by an adjacent transmission line with w_7, w_8, w_9 and w_{10}. Here five resonators are cascaded. The adjacent transmission line can be modeled as a shunt capacitor C_w,

$$C_w = \varepsilon_0 \varepsilon_r w / h$$

Where, the width of the adjacent transmission line is w and the substrate height is h. Here the dimensions are, l_1=18mm l_4=6.2mm, w_1=0.79mm w_2=0.2mm, w_3=2.6mm, w_4=0.2mm, w_5=0.4mm, w_6=0.2mm, w_7=0.7mm, w_8=1.4mm, w_9=2.1mm, w_{10}=2.8mm, x=0.2mm and g=0.2mm.

The value for the equivalent circuit elements of each separate resonator are,

$$L_s = 6.943 \text{ nH}$$

$$C_g = 0.057 \text{ pF}$$

$$C_{ps} = 2.353 \text{ pF}$$

$$C_p' = 0.837 \text{ pF}$$

$$C_g' = 0.3149 \text{ pF}$$

And $C_{w1} = 0.3328 \text{ pF}$, $C_{w2} = 0.6656 \text{ pF}$, $C_{w3} = 0.9984 \text{ pF}$, $C_{w4} = 1.3312 \text{ pF}$.

So the equivalent circuit becomes,

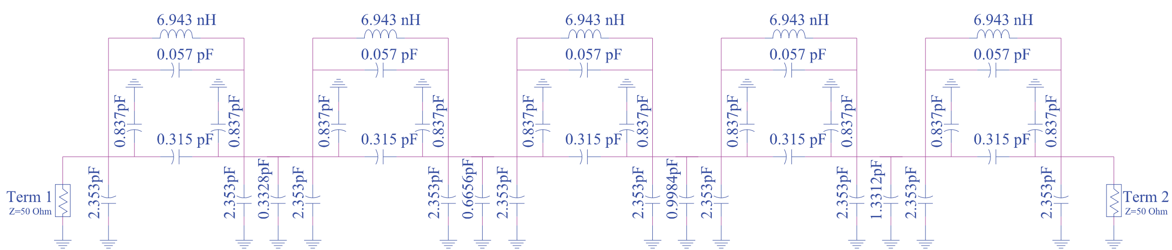

Figure 5.5 Equivalent circuit for the filter in Figure 4.11

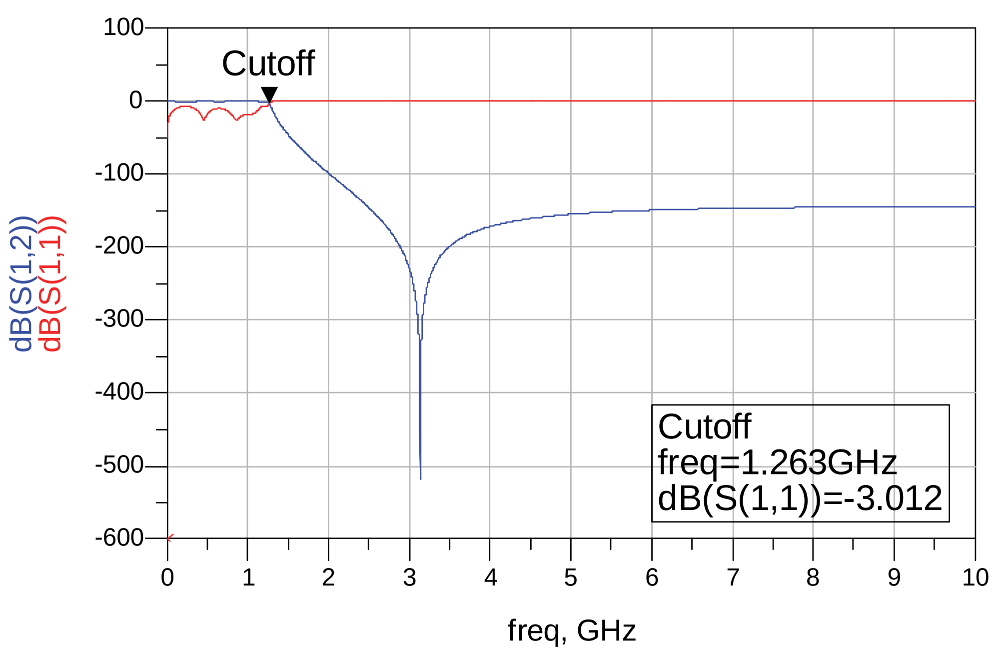

Figure 5.6 Output of the equivalent circuit of Figure 5.5

The S_{11} and S_{12} parameter of the equivalent circuit is shown in Figure 5.6. Here the cut-off frequency is found 1.263GHz which is almost equal to the cut-off frequency (1.286GHz) found from layout simulation. The rejection rate is 99dB/GHz, which is also very close to the rejection rate found in layout simulation(91dB/GHz). The rejection at stopband is found to be -145dB which is much higher than the result found in layout simulation (-85dB). We cannot approximate the higher order resonant pole-zeroes with this simplified circuit as we use the first order pi-model to find the equivalent circuit. So the equivalent circuit can accurately give the cut-off frequency and rejection rate, but fails to give the stopband rejection for the filter.

5.2.3 Cascaded proposed modified SIR hairpin filter varying length

For cascaded modified stepped impedance hairpin resonators with variable length, let two resonators are linked with by an adjacent transmission line with w_7. Here we cascade six modified stepped impedance resonator varying their length, keeping the width same. The length are varied in such a way that length of the hairpins are 48mm, 32mm, 22.4mm, 16mm, 12.8mm and 8mm. The adjacent transmission line can be modeled as a shunt capacitor C_w, where $C_w = \varepsilon_0 \varepsilon_r w / h$

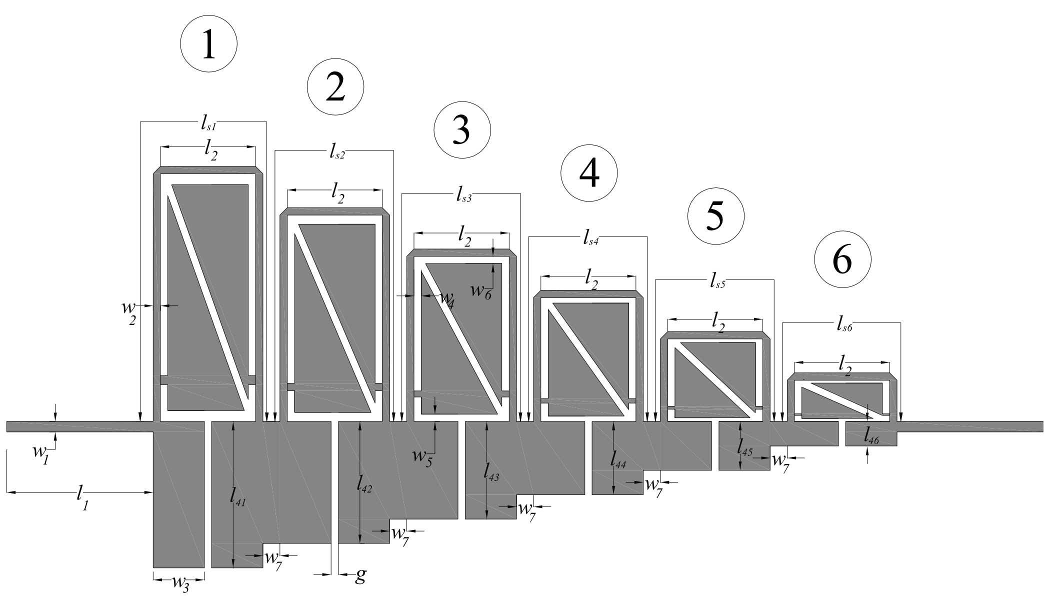

Figure 5.7 Layout of cascaded modified SIR with variation of length

The individual equivalent circuits are given by,

For length=48mm	For length=32mm	For length=22.4mm
$L_s = 10.253$ nH	$L_s = 10.925$ nH	$L_s = 9.0242$ nH
$C_g = 0.22147$ pF	$C_g = 0.1253$ pF	$C_g = 0.08275$ pF
$C_{ps} = 9.268$ pF	$C_{ps} = 5.1495$ pF	$C_{ps} = 3.3863$ pF
$C'_p = 3.1557$ pF	$C'_p = 1.9965$ pF	$C'_p = 1.301$ pF
$C'_g = 1.1869$ pF	$C'_g = 0.7509$ pF	$C'_g = 0.4893$ pF
And, $C_{w1} = 0.985$ pF	And, $C_{w2} = 0.6656$ pF	And, $C_{w3} = 0.46596$ pF

For length=16mm	For length=12.8mm	For length=8mm
$L_s = 6.943$ nH	$L_s = 5.706$ nH	$L_s = 3.672$ nH
$C_g = 0.057$ pF	$C_g = 0.0456$ pF	$C_g = 0.02825$ pF
$C_{ps} = 2.353$ pF	$C_{ps} = 1.864$ pF	$C_{ps} = 1.1523$ pF
$C'_p = 0.837$ pF	$C'_p = 0.6054$ pF	$C'_p = 0.2576$ pF
$C'_g = 0.3149$ pF	$C'_g = 0.2277$ pF	$C'_g = 0.0969$ pF
And, $C_{w4} = 0.3328$ pF	And, $C_{w5} = 0.2663$ pF	

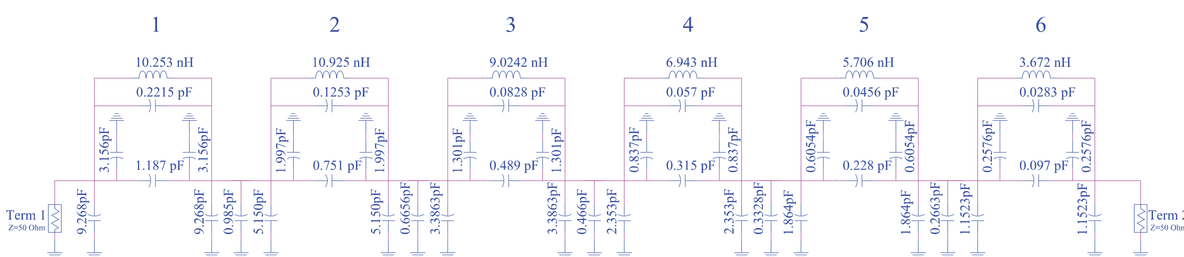

Figure 5.8 Equivalent circuit for the filter in Figure 4.13

Here from the S_{11} and S_{12} curve the cut-off frequency is found to be 565.1MHz which is close to the cut-off frequency (502.0MHz) found from layout simulation. The rejection rate is found 98dB/GHz. The rejection at stopband is found to be -170dB. Here both rejection and rejection rate found are much higher than the original value.

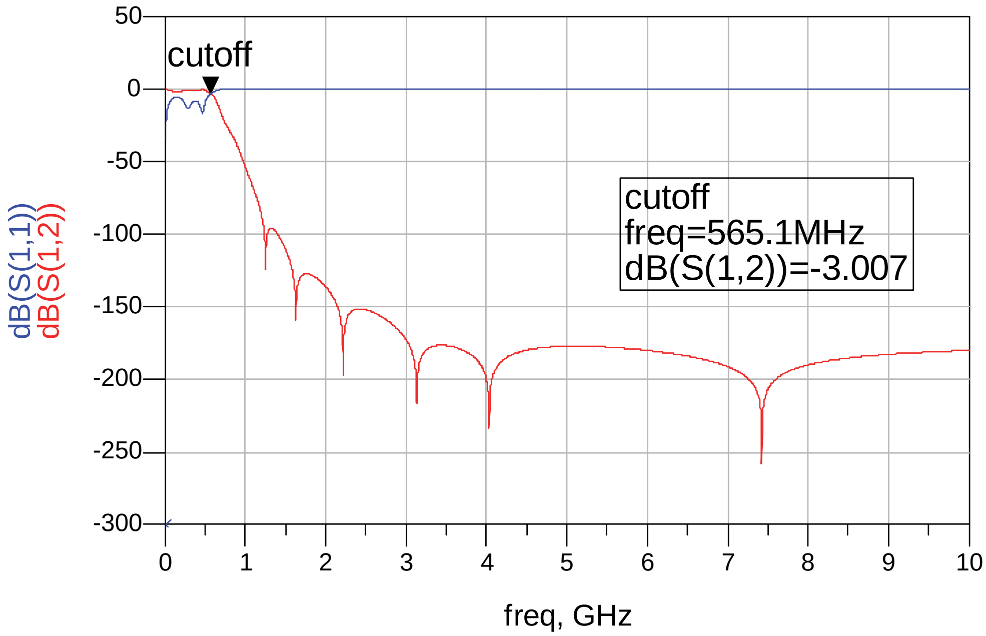

Figure 5.9 Output of the equivalent circuit of Figure 5.8

5.2.4 Single modified stepped impedance hairpin resonator varying length

For the proposed modified stepped impedance resonator filter described in section 4.3.4 where, l_1=18mm, l_2=5mm, l_3=6.1mm, l_4=6.2mm, l_5=1mm, l_6=7.3mm, w_1=0.79mm, w_2=0.2mm, w_3=2.6mm, w_4=0.2mm, w_5=0.4mm, w_6=0.2mm and gap size x=0.2mm and g=0.2mm, using the (5.1)-(5.7) the equivalent circuit becomes,

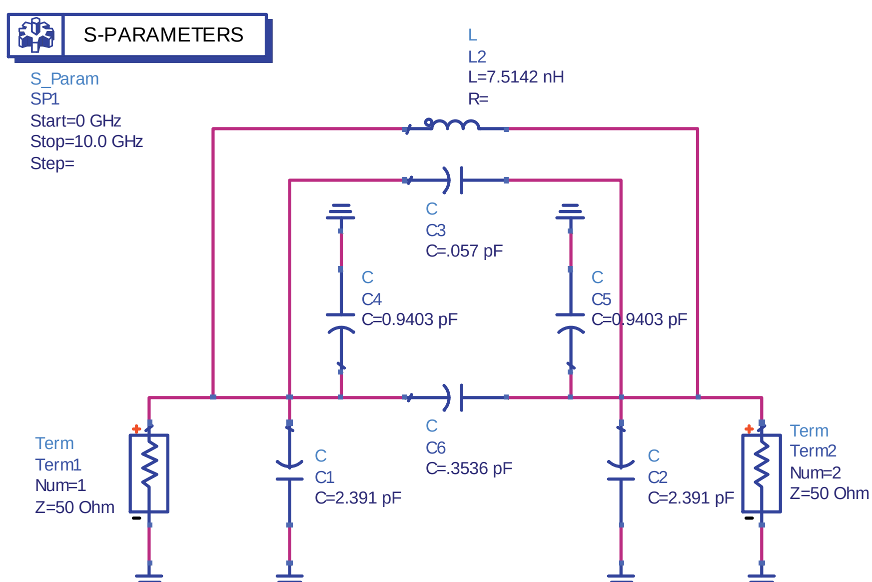

Figure 5.10 Equivalent circuit for the filter in Figure 4.15

The S_{11} and S_{12} of the equivalent circuit is shown in the Figure 5.10. It has the cut-off frequency at 1.341GHz. As we used the first order Pi-model with modified capacitance (gap-capacitance), we cannot approximate the higher order resonant pole-zeroes with this simplified circuit. Here, from the figure we find that the rejection rate is 33dB/GHz, and at stopband the rejection is of -32dB.

So the equivalent circuit show good approximation with the layout simulation for cutoff frequency, rejection rate and stopband rejection.

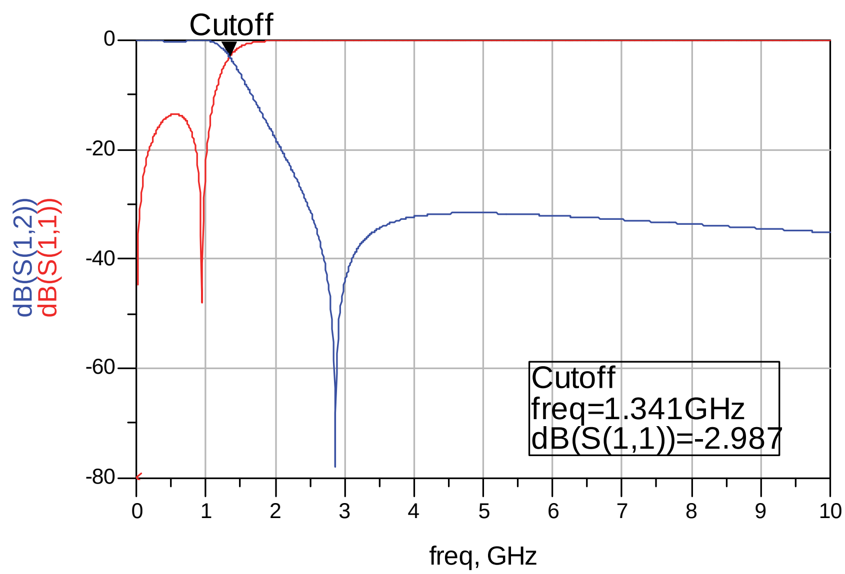

Figure 5.11 Output of the equivalent circuit of Figure 5.10

5.2.5 Single modified stepped impedance hairpin resonator varying width

For the proposed modified stepped impedance resonator filter described in section 4.3.5 where, , l_1= 18mm and w_1=0.79mm for a 50Ω feed line to match the input and output port, l_2= 4.2mm, l_3= 5.3mm, l_4=6.2mm, l_5= 1mm, l_6= 6.5mm, w_2=0.2mm, w_3=2.2mm, w_4=0.2mm, w_5=0.4mm, w_6=0.2mm, x=0.2mm and gap size g=0.2mm., using the (5.1)-(5.7) the equivalent circuit becomes,

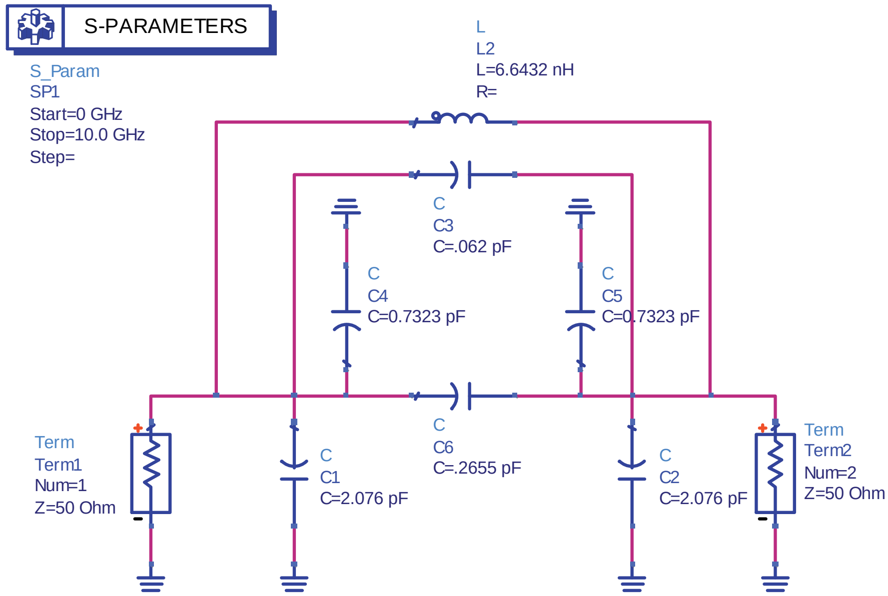

Figure 5.12 Equivalent circuit for the filter in Figure 4.17

The S_{11} and S_{12} of the equivalent circuit is shown in the Figure 5.13. It has the cut-off frequency at 1.562GHz. Here, from the figure we find that the rejection rate is 27dB/GHz, and at stopband the rejection is of -32dB.

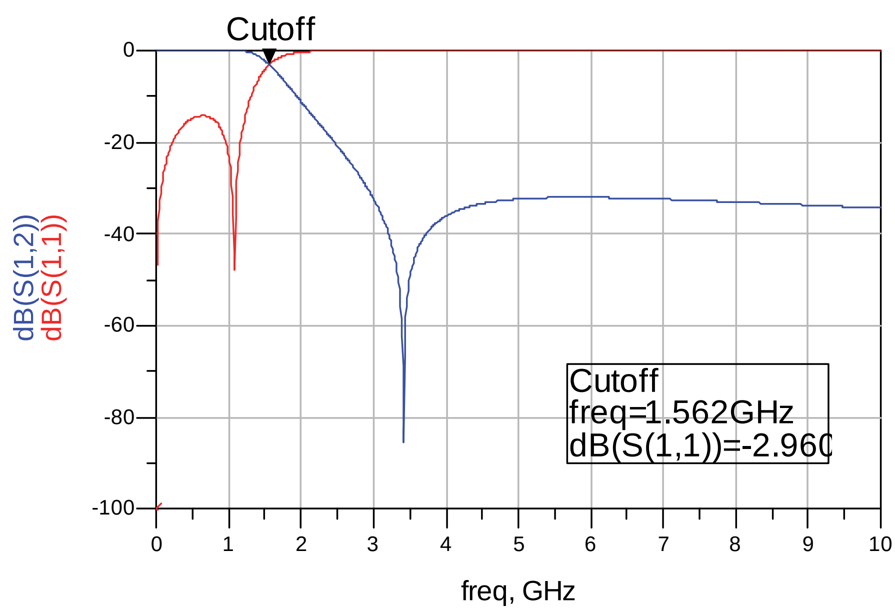

Figure 5.13 Output of the equivalent circuit of Figure 5.12

5.2.6 Single modified stepped impedance hairpin resonator varying gap

For the proposed modified stepped impedance resonator filter described in section 4.3.6 where, l_1=18mm, l_2=5mm, l_3=5.3mm, l_4=6.2mm, l_5=1mm, l_6=6.5mm, w_1=0.79mm, w_2=0.2mm, w_3=2.6mm, w_4=0.2mm, w_5=0.4mm, w_6=0.2mm and gap size x=0.4mm g=0.4mm, using the (5.1)-(5.7) the equivalent circuit becomes,

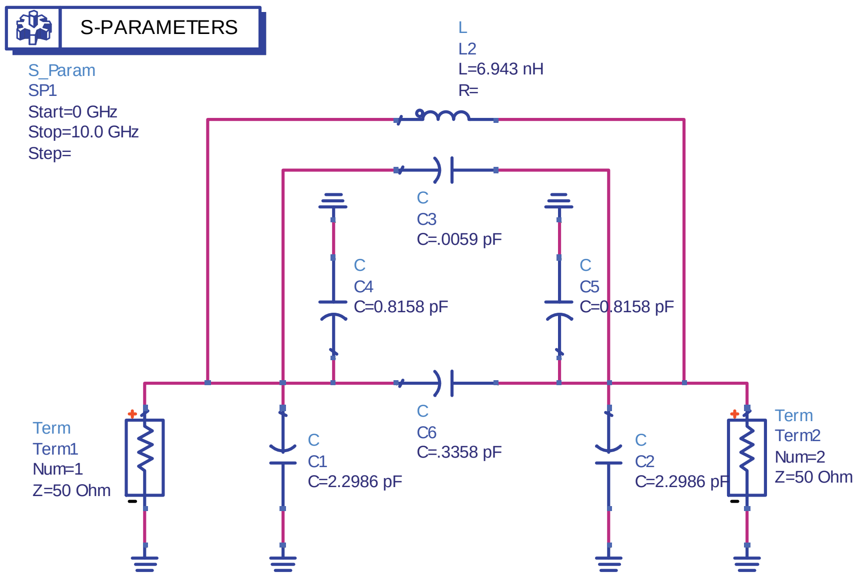

Figure 5.14 Equivalent circuit for the filter in Figure 4.19

The S_{11} and S_{12} of the equivalent circuit is shown in the Figure 5.15. It has the cut-off frequency at 1.461GHz. Here, from the figure we find that the rejection rate is 27dB/GHz, and at stopband the rejection is of -35dB.

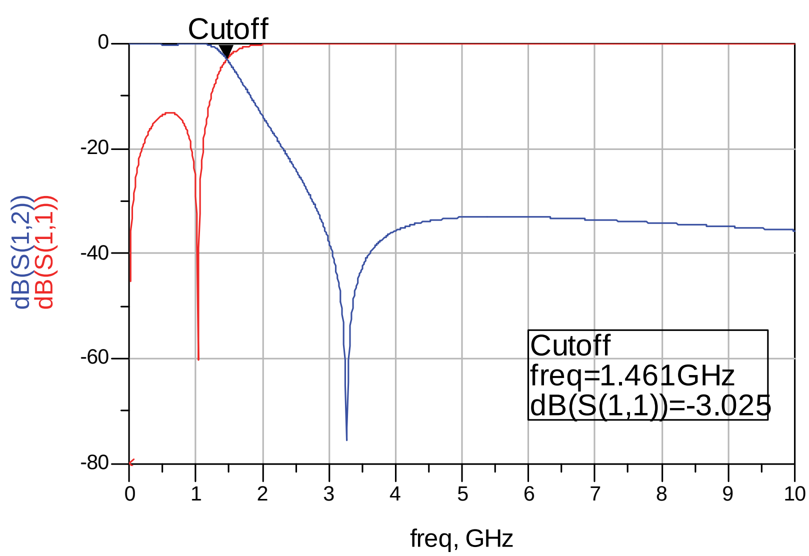

Figure 5.15 Output of the equivalent circuit of Figure 5.14

5.2.7 Single modified stepped impedance hairpin resonator adjusting for high frequency

For the proposed modified stepped impedance resonator filter described in section 4.3.6 where, l_1=18mm, l_2= 2.2mm, l_3= 1.4mm, l_4=2mm, l_5= 1mm, l_6= 2.6mm, w_1=0.79mm, w_2=0.2mm, w_3=1.2mm, w_4=0.2mm, w_5=0.4mm, w_6=0.2mm and gap size g=0.2mm, x= 0.1mm using the (5.1)-(5.7) the equivalent circuit becomes,

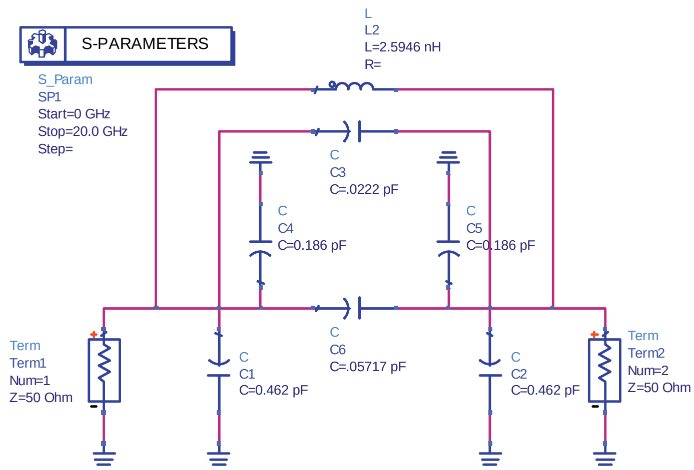

Figure 5.16 Equivalent circuit for the filter in Figure 4.21

The S_{11} and S_{12} of the equivalent circuit is shown in the Figure 5.17. It has the cut-off frequency at 4.925GHz. Here, from the figure we find that the rejection rate is 6dB/GHz, and at stopband the rejection is of -29dB.

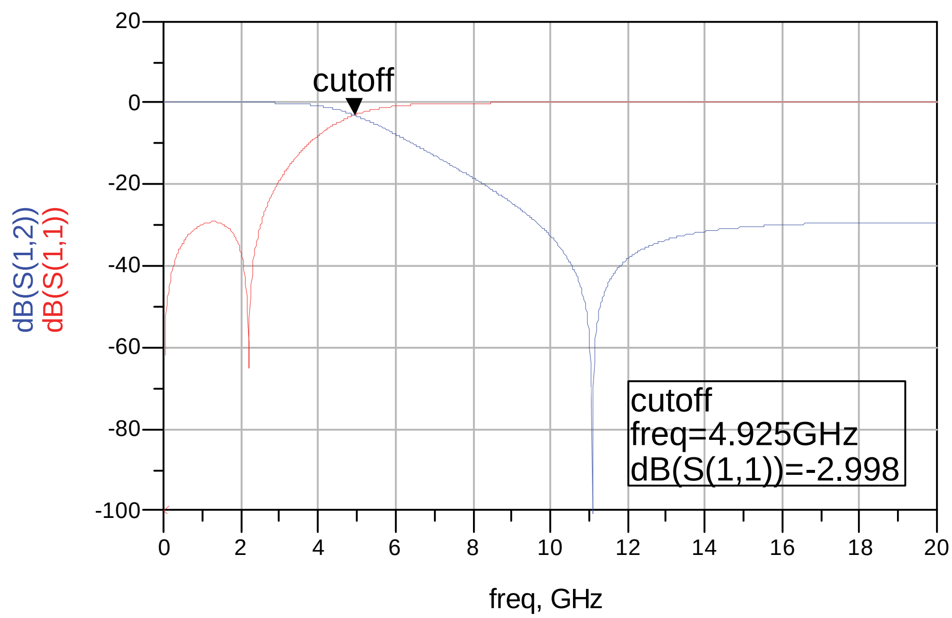

Figure 5.17 Output of the equivalent circuit of Figure 5.16

5.3 Conclusion

In this chapter the equivalent circuit for the proposed microwave filter is evaluated and verified. For all the cases it shows very good approximation to the layout simulation. It can accurately give the cut-off frequency. These circuit simulations were done in Agilent Advanced Design System 2011.01. The simulation time required for the circuit simulation is almost negligible to the time required for layout simulation using MoM.

CHAPTER 6

RESULTS AND DISCUSSION

6.1 Introduction

In order to evaluate the performance of the proposed filter and its equivalent circuit some comparison has been made. In this chapter, these comparisons are discussed and reviewed. The cut-off frequency, simulation time, compactness and suppression of the spurious effect are discussed here.

6.2 Approximation of Cut-off Frequency

The comparison between the cut-off frequency and rejection rate of the layout simulation and circuit simulation is compared in Table 6.1. From this data it is seen that for single SIR filter the circuit model derives the cut-off frequency and rejection rate are within ±4% error. But for the cascading the filter varying length, the cut-off frequency rate gives an error of -12.55%. But the rejection rate of all the filter can be estimated within ±8% error range with the equivalent circuit model.

Table 6.1 Comparison of Cut-off frequency and rejection rate of layout simulation and equivalent circuit

Sl.	Ref.	Cut-off frequency			Rejection rate		
		from layout simulation (GHz)	from equivalent circuit (GHz)	% difference	from layout simulation (dB/GHz)	from equivalent circuit (dB/GHz)	% difference
1	4.3.1 5.2.1	1.488	1.441	3.16%	27.8	27	2.88%
2	4.3.2 5.2.2	1.27	1.263	0.55%	96.2	99	-2.91%
3	4.3.3 5.2.3	0.502	0.565	-12.55%	105	98	6.67%
4	4.3.4 5.2.4	1.389	1.341	3.46%	30.7	33	-7.49%
5	4.3.5 5.2.5	1.623	1.562	3.76%	29	27	6.90%
6	4.3.6 5.2.6	1.518	1.461	3.75%	25	27	-8.00%
7	4.3.7 5.2.7	5.00	4.925	1.5%	9	6	-33.3%

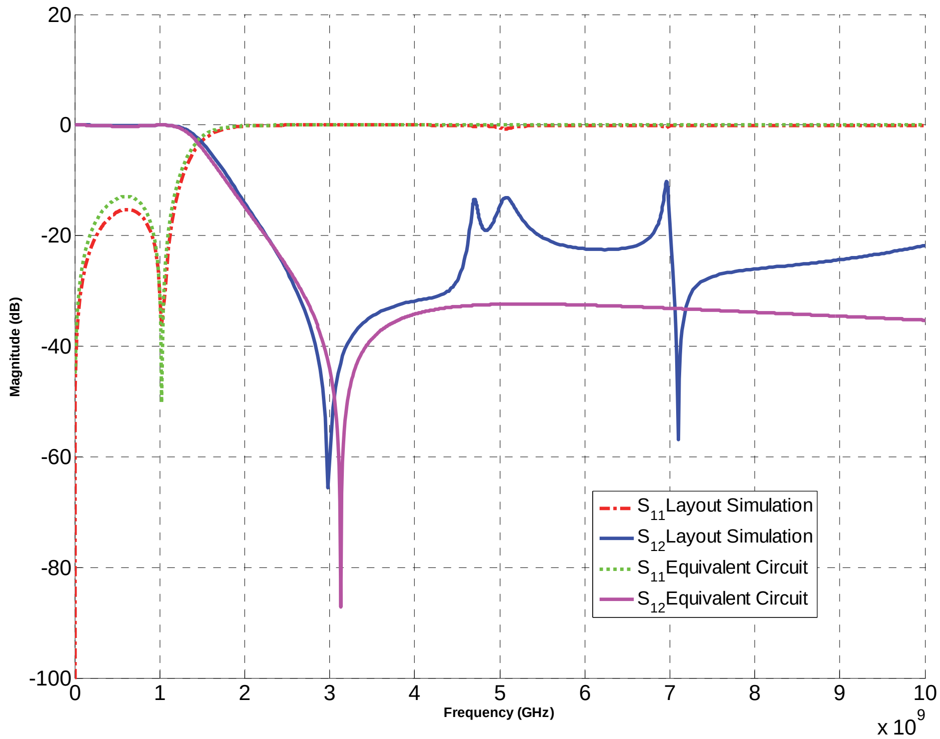

Figure 6.1 Comparison between layout simulation and equivalent circuit simulation of filter shown in Figure 4.9

To compare the result of equivalent circuit with the layout simulation, both results from Figure 5.3 and Figure 5.10 are shown in Figure 6.1. From this figure it can be seen that the cut-off frequency almost matches exactly. The passband region found from circuit simulation is almost same as the passband found from FEM/MoM simulation. The higher order harmonics do not match as we use first order L-C circuit to derive equivalent circuit.

6.3 Improvement in Simulation Time

The simulation time for the layout simulation and the circuit simulation is compared in table 6.2. From the data, it is seen that the simulation time required for the circuit simulation is about one thousandth to one hundredth of the time required for layout simulation. So the circuit simulation is essentially very helpful to minimize the designing time.

Table 6.2 Comparison of simulation time of layout simulation and equivalent circuit

Sl.	Ref.	Simulation time required		
		for layout simulation (seconds)	for equivalent circuit (seconds)	% time required of layout simulation
1	4.3.1 5.2.1	52	0.38	0.73 %
2	4.3.2 5.2.2	428	0.37	0.086 %
3	4.3.3 5.2.3	374	0.35	0.094 %
4	4.3.4 5.2.4	63	0.39	0.619 %
5	4.3.5 5.2.5	38	0.37	0.973 %
6	4.3.6 5.2.6	42	0.36	0.857%
7	4.3.7 5.2.7	37	0.31	0.838%

*Simulation is done on a Intel Core i3 machine, 4GB RAM running windows 7 64bit with the Agilent ADS (Advanced Design System) 2011.01 simulator [23].

6.4 Suppression of the Spurious Effect

From comparing the S_{11} and S_{12} of a single structure proposed by K. Cheng [1] in Figure 4.2 with the S_{11} and S_{12} of a single structure proposed in this thesis in Figure 4.10, It is seen that the spurious effect is drastically reduced. This is due to the inclusion of the triangular coupled capacitance added in the proposed structure. For K. Cheng's filter the stop-band bandwidth is 4.09GHz (1.86GHz to 5.95GHz). On the other hand the stop-band bandwidth of the proposed filter in this thesis is 10.512GHz (1.488GHz to 12.00GHz).

6.5 Compactness of the Structure

In this section the size of the proposed filter is compared with the size of the filter proposed by K. Chang [1] for the same frequency. The frequency considered here are 1.4GHz, 1.5GHz, 1.6GHz, 1.7GHz, 1.8GHz, 1.9GHz and 2.0GHz. The measured result is shown in Table 6.3. From this data it is found that, for same cut-off frequency and

0.254mm thick RT/Duroid 5880 substrate with a relative dielectric constant ε_r=2.2, the proposed filter in this thesis is roughly about 30% smaller than the filter proposed by K. Cheng. So the proposed structure is more compact than any other SIR filter proposed before.

Table 6.3 Comparison of size of proposed filter and filter proposed by K. Cheng [1]

Case	Frequency (GHz)	Size		
		Kai Cheng Model (mm^2)	Proposed model (mm^2)	% size of Kai Cheng Model
1	1.4	**114** (7.6 × 15.0)	**79.46** (5.8 × 13.7)	**69.70**
2	1.5	**102.9** (7.0 × 14.7)	**72.9** (5.4 × 13.5)	**70.85**
3	1.6	**93.84** (6.8 × 13.8)	**66.5** (5.0 × 13.3)	**70.87**
4	1.7	**82.8** (6.0 × 13.8)	**60.26** (4.6 × 13.1)	**72.78**
5	1.8	**77.14** (5.8 × 13.3)	**54.6** (4.2 × 13.0)	**70.78**
6	1.9	**71.28** (5.4 × 13.2)	**49.4** (3.8 × 13.0)	**69.30**
7	2.0	**63** (5.0 × 12.6)	**44.45** (3.5 × 12.7)	**70.56**
8	5.0	**18.2** (2.8 × 6.5)	**14.04** (2.6 × 5.4)	**77.14**

6.6 Summary

In this chapter, the performance of the proposed microstrip filter is evaluated in different aspects. At first the performance of the equivalent circuit is compared with the FEM simulation results of the proposed filters. Then the performance of the proposed filter is compared with the filter proposed by K. Cheng. From these evaluations, it is found that the proposed method gives a better performance than existing methods. These results has been published in [24].

CHAPTER 7

CONCLUSION

7.1 Conclusion and Discussion

In this thesis, the first order transmission line model is used. So it cannot approximate the higher order spurious modes. But the cut-off frequency, rejection rate and the passband ripple is accurately approximated. If the higher order of the transmission line is used then a more close approximation can be achieved. But for higher order transmission line, mathematical derivation will become very difficult.

Although the layout simulation is more accurate, it is not always convenient to use because for large cascaded circuits it takes too much time for completing the simulation. So at initial stage of a filter designing the layout simulation is not a practical solution. Designer can roughly calculate the cut-off frequency, rejection rate and stop band rejection from the equivalent circuit. This drastically reduces the time to complete the design. When the required parameters are roughly found, then finally the layout simulation can be done to get the exact accurate result.

From Table 6.3, it is found that the proposed filter is about 30% smaller than previously proposed similar filters. So a very good compactness is achieved here, which is one of the main requirements of designing a filter.

7.2 Scope of Further Work

There are a number of scopes to extend the research done in the thesis. Some possible avenues are:

- For deriving the equivalent circuit the first order transmission line equivalent circuit is used in this thesis. So the higher order spurious modes cannot be found from the equivalent circuit. If the higher order of the transmission line is used then a more close approximation can be achieved.
- To reduce the spurious effects, some novel elements such as Photonic crystal or metamaterial can be used with the proposed filter.

- The proposed filter can be actually fabricated and the measured data can be compared with the simulated results.
- In this thesis the lowpass filter is designed. But Integrating multiple number of the proposed filter, a narrow bandpass filter can be designed.

REFERENCES

[1] Hsieh, L. H. and K. Chang, "Compact, broad-stopband elliptic-function lowpass filters using microstrip stepped impedance hairpin resonators," *IEEE MTT-S International Microwave Symposium*, 1775-1778, Philadelphia, USA, June 2003.

[2] Ju-Hyun Cho, Jong-Chul Lee, "Compact microstrip stepped-impedance hairpin resonator low-pass filter with aperture," *Microwave and Optical Technology Letters*, Volume 46, Issue 6, pages 517–520, 20 September 2005.

[3] Cheng-Liang Huang, Cheng-Hsing Hsu, Chih-Ming Tsai, "Miniaturization of hairpin bandpass filters using high-permittivity substrate," *Microwave and Optical Technology Letters*, Volume 45, Issue 3, pages 222–225, 5 May 2005.

[4] Yu-Wei Chen, Min-Hua Ho and Yen-Ju Liu, "The design of a compact quasi-elliptic filter using stepped impedance resonators with harmonic suppression," *Microwave and Optical Technology Letters*, Volume 49, Issue 4, pages 800–804, April 2007.

[5] Yang, M. H. and J. Xu, "Design of compact, broad-stopband lowpass filter using modified stepped impedance hairpin resonators," *IEE Electron. Letter*, Vol. 44, No. 20, 899-900, 2008.

[6] Cheng-Hsing Hsu Hsu, C.-I.G. Hsuan-An Ho , "Hybrid microstrip compact hairpin bandpass filter," *Microwave Conference, 2009. APMC 2009. Asia Pacific*, Issue Date 7-10 Dec. 2009 page(s): 2505-2507,Singapore.

[7] Sagawa, M., K. Takahasi, and M. Makimoto, "Miniaturized hairpin resonator filters and their application to receiver front-end MIC's," *IEEE Trans. Microwave Theory Tech.*, Vol. 37, No. 10, 1991-1997, 1989.

[8] Kuo-Sheng Chin, Deng-Jun Chen, "Harmonic-suppressing bandpass filter based on coupled triangular open-loop stepped-impedance resonators," *Microwave and Optical Technology Letters*, Volume 52, Issue 1, pages 187–191, January 2010.

[9] Jia-Sheng Hong, M. J. Lancaster, "Microstrip Filters for RF/Microwave Applications," *John Wiley & Sons, INC.*, A Wiley-Interscience publications.

[10] H. R. Chuang, J-W. Huang, C.C. Wei, Jason L. C. Chang, "3D FEM simulation and experimental measurement dielectric-resonator filters" *Microwave and Optical technology letters*, Vol. 8, pp. 196-200, March 1995.

[11] G. Leon, R. R. Boix, F. Medina, "Tunability and bandwidth of microstrip filters fabricated on magnetized ferrites," *Microwave and Wireless Components Letters*, Vol. 14, pp. 171, 2004.

[12] G. C. Temes, and S. K. Mitra, "Modern Filter Theory and Design," *Wiley*, New York, 1973.

[13] J. D. Rhodes, "Theory of Electrical Filters," *Wiley*, New York, 1976.

[14] L. Weinberg, "Network Analysis and Synthesis," *McGraw-Hill*, New York, 1962.

[15] A. Papoulis, "*The Fourier Integral and Its Applications,*" McGraw-Hill, New York, 1962.

[16] K. C. Gupta, R. Garg, I. Bahl, and P. Bhartis, "Microstrip Lines and Slotlines," *Artech House*, Second Edition, Boston, 1996.

[17] E. O. Hammerstard, "Equations for microstrip circuit design," in *Proceedings of the European Microwave Conference,* Hamburg, Germany, 1975, pp. 268–272.

[18] E. O. Hammerstad and O. Jensen, "Accurate models for microstrip computer-aided design," *IEEE MTT-S,* 1980, Digest, pp. 407–409.

[19] Garg, Ramesh and I.J Bahl, "Microstrip discontinuities," *International Journal of Electronics,* Vol.45, No. 1, 1978, pp. 81-87.

[20] Hoffman, Reinmut, "Handbook of Microwave Integrated Circuits," *Artech House*, Norwood, MA, 1987.

[21] Brian C. Wadell, "Transmission Line Design Handbook," *Artech House*, Norwood, MA, 1987, pp. 330-332.

[22] George I. Zysman, "Coupled transmission line networks in an inhomogeneous dielectric medium," *IEEE Transaction on microwave theory and technique*, Vol MTT-17, No. 10, 1969.

[23] Agilent Advance Design System version 2011.1 url: http://www.agilent.com.

[24] Sayed Ashraf Mamun, Md. Abdul Matin, "Modeling of compact, broad-stopband lowpass filter using modified stepped impedance hairpin resonators," *International Journal of Computer and Electrical Engineering*, Vol. 3, No. 6, 2011.